British Geological Survey

OVERSEAS DIRECTORATE

LINEAMENT STUDIES IN MASVINGO PROVINCE, ZIMBABWE

D. Greenbaum

Natural Environment Research Council

Report MP/87/7/R
British Geological Survey
Keyworth
Notts UK
31 March 1987

BRITISH GEOLOGICAL SURVEY

Overseas Directorate

LINEAMENT STUDIES IN MASVINGO PROVINCE, ZIMBABWE

D Greenbaum

Natural
Environment
Research
Council

WC/
Report MP/87/7/R
British Geological Survey
Keyworth
Notts, UK, NG12 5GG

31 March 1987

SUMMARY

This report describes the results of structural investigations carried out in Masvingo Province, SE Zimbabwe between April 1986 and March 1987 as part of a continuing study of groundwater in crystalline basement rocks. An analysis has been made of lineaments interpreted from enhanced Landsat multispectral scanner imagery and aerial photographs, in conjunction with field studies of fractures (joints and faults) and dykes. Descriptions are given of the geological setting and brittle stuctures in 14 sub-areas selected to provide a cross-section of the geology in areas showing a high incidence of low- and in part high-yielding boreholes. Preliminary analysis of the field data indicates only a partial correlation between major lineament directions and steep, closed joints typical of most granitic outcrops: it is likely that these are related to residual stresses released during erosional unloading. A better correlation is seen between lineaments and older quartz-cemented shears or minor faults. The main lineaments form several well-grouped sets that can be correlated with important igneous-tectonic events in the craton. Four main compressive-tectonic events are recognised in post younger granite times whose directions of shearing indicate a rotation in the maximum horizontal principal stress vector from about NNW-SSE to WNW-ESE. Analysis of this data is continuing. Comments are also offered regarding borehole siting procedures. It is noted that whereas these rely heavily on the photogeological detection of lineaments, they suffer from a number of constraints (socialogical and logistical) that may be at least partly responsible for the poor borehole success rate in some areas. Finally, structural aspects of the future work programme are discussed.

1. INTRODUCTION

Previous structural studies in the Masvingo region looked at the role of remote sensing in hydrogeology (Greenbaum 1985) and discussed the brittle deformation history of the region based on published reports and a preliminary analysis of Landsat imagery (Greenbaum 1986a). This latter study recognised several episodes of Late Archaean/Proterozoic brittle deformation and dyke emplacement.

Following these studies a number of areas (A to N) were identified, based on a high incidence of low- and in some cases high-yielding boreholes across a range of rock types (Figure 1), for detailed investigation. During the current year structural work has concentrated on the following aspects:

(i) an analysis of photolineaments from 1:25,000 and 1:80,000 aerial photographs;

(ii) the examination of fractures in outcrops;

(iii) observations on current borehole siting procedures;

(iv) the selection of sites for geophysical investigations.

A short report was prepared in July 1986 at the conclusion of the field programme summarising general findings and suggesting sites for follow-up geophysical studies (Greenbaum 1986b).

From a structural viewpoint it was hoped the geophysical programme would provide answers to the following:

- are the geophysical techniques employed able to confirm the presence of a fracture or dyke and what information can they provide as to its width and that of any associated zone of weathering?

- do the results indicate differences in the nature of fractures at high- and low-yielding boreholes?

- with what degree of accuracy can the methods locate the position of steep structures under different geological conditions?

- what are the limitations of the techniques and what are the likely ambiguities in the interpretation?

In a number of cases the aim of a suggested site investigation was to provide further information on an inferred fracture or dyke. At time of writing, the results of the geophysical work are not available so that conclusions relating to this aspect of the work will have to be considered at a later stage.

In addition, further work remains in the following general areas: (i) correlation studies between lineaments and borehole parameters; (ii) more detailed analysis of fracture directions measured at outcrops; and (iii) further photogeological interpretation of lineaments in the vicinity of borehole sites.

2. PROCESSING OF REMOTE SENSING DATA

The interpretation of Landsat MSS imagery and aerial photography was continued and extended during the present phase of the project, and an analysis carried out of the resulting lineament datasets. Aerial photographs at a scale of 1:25,000 were obtained for all detailed study areas and full regional coverage at 1:80,000. Due to the size of the area only a 'rapid' interpretation of the photographs was feasible.

The majority of lineaments are observed over areas of outcrop and are manifested either as negative relief features or as sharply defined linear traces: they have the appearance of fractures (faults or joints). Over areas of regolith, lineaments are less apparent. They are marked by drainage patterns, vegetation lines and changes in tone (e.g. soil moisture content), and relate to both fractures and dykes. Because some of the more subtle lineaments over regolith may have been missed in the rapid area studies, some further photogeological work in the vicinity of specific borehole sites may be needed before correlation studies are undertaken.

The large aerial photograph dataset (approximately 14,000 lineaments from a total of 14 study areas) required a rapid method of transfer of lines to a geometrically corrected base. The following procedure was adopted. Each aerial photograph, with interpreted lineaments marked in red, was photoreduced in two stages on a plain paper ('Xerox') copier to a scale of approximately 1:50,000. By optimally adjusting the contrast setting it was found possible to obtain a final photocopy that retained sufficient topographic detail for it to be matched with the topographic map over a light table. By 'juggling' the position of each photocopy to obtain the best local fit (within the limitations of the radial and relief distortion inherent in

the photograph), lineaments could be traced off with reasonable accuracy: error for an individual lineament was estimated to be not more than 200 metres. The photocopying technique was also used to make up crude photolaydowns (mosaics) which were found useful for providing an overview of the structural grain of the country, a feature not usually evident at the scale of a single photograph.

Lineaments were digitised from the resulting 1:50,000 topographic maps and written to files on the Keyworth GEC 4090 computer. Following editing and reformatting, separate files for each detailed study area were generated, each consisting of pairs of x-y co-ordinates corresponding to lineament end points. Several previously written programmes were upgraded for processing of the Zimbabwe dataset. For each detailed area, separate plots were produced of lineaments and of lineament density (in units of total length/area) at a scale of 1:50,000 on film and at 1:100,000 on paper (Figures 2A - N & 3A - N). Corresponding rose diagrams are shown in Figures 4A - N. Lineaments were classified as either fractures or dykes and digitised under separate codes. For all sub-areas except E plots are for fracture data only. Area E includes dykes as these make up a significant proportion of linaments. (Plots for other areas that include dykes will be generated later). Figure 5A is a rose diagram for the summed photolineament dataset.

Lineaments interpreted from Landsat imagery (scenes 169-74 and 170-74) were digitised and processed in a similar way. Figure 5A is a rose diagram of this data and Figure 6 a plot at a scale of 1:2,000,000.

3. STRUCTURAL ANALYSIS

In this section the relationships between lineaments determined by remote sensing and fractures measured on outcrops are considered in relation to the geology of the study areas. The analysis of the fracture data is continuing and conclusions presented here are therefore preliminary.

3.1 Descriptions of detailed study areas

Area A: Gneissic, coarse-grained granite belonging to the Zimbabwe Granite forms bornhardt terrain over the northern half of the area. To the south older gneisses give rise to a low lying area of thicker regolith and poor exposure.

On satellite imagery, long fractures of the NNW set are evident in the north of the area and appear to pass into a broad, somewhat diffuse shear zone southwards: on aerial photographs and on the ground this zone up to several kilometres wide is represented as an area of low relief with few outcrops.

Photolineaments are most abundant in the Zimbabwe Granite, comparatively few occurring in the gneisses to the south. The lineament plot (Figure 2A) and rose diagram (Figure 4A) show a preponderence of directions between 60° and 80° with swarms of lineaments varying systematically in direction from one part of the area to another. In the field these directions correspond to a mineral foliation (gneissosity) dipping steeply to the south, parallel to which joints are developed (Plate 1). This mineralogical anisotropy has controlled the erosion form of many bornhardts (Greenbaum 1986a).

Other common directions are between 310° and 20° and appear to

include several discrete sets, notably 340°, 15° and 355°. Field measurements on outcrop confirm the presence of several sets of NW to N closed vertical joints and occasional quartz-filled veins trending NNW and WNW.

Area B: This area lies within the Northern Marginal Zone (NMZ) of the Limpopo Mobile Belt and displays a strong ENE regional fabric. Migmatitic gneisses are intruded by stocks of coarse porphyritic granite in central and northeast part of the area and by ENE-trending sheet-like bodies of mafic granulite in the southeast.

Two fracture directions are prominent (Figures 2B &4B). The dominant set is in the range 310° to 350° with an average of about 330°: it may comprise two or more fracture sets. A second direction averages 70°, parallel to the regional structural trend. This set is best developed in the strongly deformed granulites to the southeast. Lineaments trending NNE also occur in this southeast corner: they are part of series of long faults mapped in this area (Robertson 1974) and evident on Landsat imagery.

The rocks of area B were found to be the least fractured of all areas studied. It would seem that here stresses were resolved along major fractures in such a way that the intervening rock masses remained largely unaffected. Outcrops form smooth domes and bornhardts, erosion taking place predominantly by sheet exfoliation (Plate 2). Where fractures were noted their directions showed reasonable correlation with lineaments seen on the aerial photographs. Northwesterly directions were found to correlate mainly with closed vertical joints. NNE fractures were among other prominent though less common directions. Possible conjugate shear joints were measured at two localities indicating a horizontal principal stress oriented at about 300°. Only occasional evidence was seen of fractures parallel

to mineral foliation; this is nevertheless regarded as the principal control of the ENE fractures evident on photographs.

Area C: This area includes several rock formations. The southern margin of the Chibi Granite is exposed in bornhardt terrain in the north of the area while small, isolated stocks of younger granite form spectacular domes in the southeast. Elsewhere the older gneisses give rise to low relief terrain. The Buchwa greenstone belt forms a range of hills that traverse the area centrally from WSW to ENE.

The dominant trend of lineaments in this area, as determined from both satellite imagery and aerial photographs, is NNW (Figures 2C & 4C). Subsidiary directions are WNW and ESE.

In the field, the migmatitic gneisses are strongly banded and often contorted: mineral foliation trends ENE. These rocks are poorly exposed but wherever seen do not appear to be strongly fractured. The main directions are NW to NNW. Near Rungai in the southeast of the block, stocks of gneissic granite, emplaced into the migmatic gneisses, form a group of large bornhardts the margins of which are controlled by the ENE mineral foliation and a series of closed planar vertical joints striking about 325°. On Rungai hill itself closed planar fractures of this set extend vertically through some 300 m and, despite their apparently insignificant expression at outcrop scale, exert a controlling influence on erosion. Major fractures along this direction isolate individual bornhardts attesting to the importance of this direction. Followed NNW towards Chikore School one of these fractures (here trending 322°) appears to displace the outcrop of the greenstone belt sinistrally some 300-400 m. A borehole located alongside this fault provides a good yield. In the NW of the area the displacement on a basic dyke (interpreted from aerial photographs) suggests a dextral sense of movement on a fault

trending 314°. Evidently, more than one set of fractures trending NW is represented in this area.

Within the Chibi Granite and in the southwest part of area C occur several WNW-trending lineaments, some of which appear to displace the greenstone belt sinistrally.

Area D: The greenstones of Mt Buchwa occupy the central part of this area. To the north and south occur areas of tonalitic gneiss.

No fieldwork was carried out in this area owing to difficulties of access. All conclusions are therfore based on remote sensing.

Satellite images show few lineaments in this area. A long, though diffuse, lineament trending 305° appears to be an extension of the Mtshingwe Fault which cuts the Great "Dyke" with major dextral displacement. Other satellite lineaments trend W to WNW and one of these shows possible sinistral displacement. The Sebanga Poort dyke and associated NNW fractures pass through the northeast corner of the area.

On aerial photographs (Figures 2D & 4D) several directions appear to be present, the main ones trending 275°, 70° and 345° although there is a considerable spread around these averages especially so far as the NNW set is concerned. The 305° fracture detected on imagery is not, however, readily apparent on aerial photographs.

Area E: This is an area of ancient gneisses and metamorphosed dolerite dykes (the ENE and WNW trending Mashaba-Chibi set) forming an area of low relief with nearly continuous (though probably thin) regolith cover. Outcrops of granitic rock are

largely restricted to river bed exposures. The rocks are strongly banded or migmatitic, pale grey, medium-grained gneisses heavily veined by quartz stringers and extensively fractured along several directions. Mineral foliation appears to be the main control of near-surface weathering. These rocks are affected by several episodes of post younger granite fracturing and dyke emplacement viz:

(i) inception of NNE (probably sinistral) fractures and infilling by dolerite (e.g. East Dyke) and quartz;

(ii) dextral movement along the ENE Jenya Fault and intrusion of dolerite along parallel fractures locally;

(iii) NNW fracturing and emplacement of the Sebanga Poort and related dykes;

(iv) ENE dextral strike-slip faulting including reactivation of older Mashaba-Chibi dykes. Dolerite intrusion and silicification.

Lineaments are moderately abundant on aerial photographs but in this area correspond to dykes more often than fractures. Figures 2E, 3E and 4E include both dykes and fractures. The older Mashaba-Chibi dykes are distinguished by darker soil tones, rubbly outcrops and commonly a vegetation line. They are often sinuous in their appearance on aerial photographs and exhibit variations in width and continuity, possibly as a result of deformation. The younger dykes are more constant in width and direction. They commonly form elevated relief features and are heavily wooded possibly as a result of the increased availability of groundwater along the dyke (Plate 3). However, the phenomenon may be in part artificial, resulting from bush not having been removed from zones of rubbly outcrop

during clearing operations. Fractures do not give rise to strong lineaments in this area but may be evident as subtle vegetation lines, darker tones (perhaps related to soil moisture) or as displacements across dykes. Fractures filled by massive quartzite form conspicuous low ridges on aerial photographs.

Owing to their relative abundance and comparative ease of identification on aerial photographs, dykes form the main target for boreholes in this area. Near Shumba School a dolerite dyke trending ENE lies across the slope of a hill and forms a natural barrier to groundwater flow. Uphill of the dyke standing water occurs in shallow excavations to within 50 cm of the surface (dry season observation), while on the downslope side seepages originating at the dyke form outwash gulleys extending downhill (Figure 7). A borehole drilled on the downhill side by Hydrotechnica (presumably to avoid contamination from surface runoff on the uphill side) proved dry.

At another location to the west of the East Dyke, a hole drilled by Hydrotechnica within 2 m of an outcropping, late, WNW-trending porphyritic olivine dolerite dyke failed to strike water. The site was chosen close to a small seep and gulley, near the base of a gentle slope: the dyke was evidently viewed as a subsurface barrier to groundwater flow and the margin of the dyke as a potentially fractured aquifer. Two further holes were drilled several hundred metres further along the same dyke. The first of these was also dry, but the final hole, again located adjacent to the dyke and towards the base of a long, gentle slope (i.e. in a very similar situation to their first attempt), provided a moderate flow.

Little consideration appears to have been given to the possibility of dykes themselves acting as aquifers. Outcropping dykes are invariably highly fractured and support a

prolific flora. They vary considerably in width from less than 2 m to more than 100 m: an inclined hole drilled through one of the larger dykes would be valuable in ascertaining the relative importance of the barrier concept, the shattering of the contact rocks and the groundwater storage capacity of the dyke itself.

Area F: The greater part of area F is occupied by the outcrop of the Chibi Granite forming spectacular bornhardt terrain. The granite batholith is bordered in the northwest by older gneisses intruded by swarms of Mashaba-Chibi dykes, forming a low-relief, regolith-covered area.

The granites are medium grained, grey to pink rocks with a moderate to well developed gneissic foliation, pervasively injected by pegmatite veins. Veins range in width from less than 1 cm to more than a metre, and are both deformed (remobilized) and undeformed: they appear to belong to several generations formed during the late emplacement (ductile) and post-emplacement (brittle) stages of the granite. Though directions vary, veins frequently occur in sets of consistent orientation, usually NNW to NE, and tend to be moderately steeply inclined. From a hydrogeological viewpoint these pegmatite veins are of potential significance since they commonly show the development of planar fractures and display strong preferential weathering.

The Chibi Granite is strongly fractured along NNE and NW to NNW dislocations of regional extent as shown on the geological map of the area and evident on Landsat images and aerial photographs. The photolineament map (Figure 2F) and rose diagram (Figure 4F) indicate that the principal direction is 335°, with subsidiary peaks at around 20° and 75°. There are also a number of lineaments between NNW and WNW.

The correlation between lineaments determined by remote sensing and fractures observable at outcrop is somewhat variable. Generally, more fracture directions are evident in the field and, not uncommonly, the most prominent photolineaments are not dominant in outcrop. This brings into question the extent to which the minor fractures (mainly joints of youthful appearance) are related to the dominant fractures that transect the craton. One possibility is that whereas the main fractures are first order dislocations directly related to the principal stresses, joints and minor faults seen within fault-bounded blocks result from residual, second and lower order stresses perhaps released during much later erosional unloading. If this is so, then such fractures cannot be used directly to infer the nature of the major lineaments determined from remote sensing. Further analysis of the field data is planned to examine these possibilities.

The dominant 335° lineament direction from aerial photographs is not conspicuous at outcrop, although at some localities a few well-developed planar joints of this orientation are seen, while at one site a quartz-filled fault showing slight sinistral movement was noted. The main directions seen are between W and NW, within which range more than one set may be represented. Most fractures of this type are again closed vertical joints of fresh appearance sometimes forming apparent conjugate shear sets (Plate 4): occasional evidence is seen of displacement (both dextral and sinistral) and of silicification.

The NNE set is conspicuous on imagery as a series of long, though widely spaced, fractures some showing apparent sinistral offset of the batholith margin. The geological map shows some of these fractures to be veined by quartz. At outcrop, NNE fractures occur as closed, planar vertical joints and as narrow (less than 0.5 cm) quartz-filled fractures. At some sites within the Chibi Granite, especially in country between areas C

and F (e.g. around Davira), many of the NNE fractures show small sinistral strike-slip displacements (Plate 5). Very occasionally within area F, are seen NNE fractures showing dextral movement which may indicate reactivation of this direction.

A prominent NNE fracture passes near to Chivurugwi old store, 2 km south of Chibi. Here, shallow pits beside the road along the line of the fracture contain standing water, and a dug well had water flowing out of it at the time of my visit during the dry season. It was said to always provide a good supply.

The NE to ENE peak on Figure 4F appears to correspond to the foliation direction within the granite and older gneisses, the strike and degree of development of which show considerable variation regionally: some of the most spectacular fracturing associated with foliation occurs in the west of the Chibi area along an E-W foliation direction. There is a suggestion from remote sensing that such variations in foliation direction result from rotations of fault-bounded blocks.

To summarise then, the main fracture directions in area F are as follows:

- NNE fractures form a set of widely spaced, strike-slip shears showing sinistral displacement and related probably to Great "Dyke"/Popoteke fracturing event. At outcrop they are seen as narrow quartz-filled and closed, joints and minor sinistral faults.

- northwesterly fractures comprise a compound set with separate NNW and NW directions represented. The NNW direction is possibly part of the Sebanga Poort set. The NW set may represent conjugate (dextral) shears related to the NNE set.

. NE to E fractures were developed along foliation.

Area G: Area G is shown on the 1:100,000 geological map as younger granite. It is an area of rounded bornhardts separated by expanses of low-lying, regolith-covered terrain. The granites are gneissic to migmatitic and are often strongly fractured along various directions. Pegmatite veins of several generations are present and again show the development of planar fractures and preferential weathering. The Popoteke Fault, here trending N, passes through the east of the area where it forms a ridge suggesting it to be silicified or intruded by dolerite.

The photolineament plot (Figure 2G) and rose diagram (Figure 4G) shows considerable dispersion with prominent peaks towards the NNW and ESE.

The correlation between fracture directions measured at outcrop and lineament directions from aerial photographs is moderate. The ESE set correlates with fractures developed along the mineral foliation. Other common fracture directions are E to NNE: they occur both as closed, planar, vertical joints and as occasional quartz-filled fractures. Near Nanwi School a linear stream course marks the location of a prominent fracture along which water discharges throughout the dry season. Bedrock is at shallow depth and the fracture can be positioned to within 2 metres between outcrops in the centre of the vlei. This therefore represents the maximum width of this fracture. The adjacent outcrops display an intense swarm of narrow quartz-filled fractures trending 340° parallel to the lineament. Evidently, late movement or erosion along the main fracture has produced significant permeability in what was probably a cemented shear.

Area H: No fieldwork was done in this area so that conclusions are based on published information and remote sensing data only.

Area H lies within the NMZ of the Limpopo Belt in an area mapped as paragneisses, containing relicts of greenstone belts, metamorphosed to granulite facies grade.

A northerly trending lineament belonging to the Great "Dyke" set is seen on Landsat imagery passing through this area. This is also evident as a series of shorter fracture traces on aerial photographs (Figure 2H) but NNW, NW and in particular ENE directions are also prominent (Figure 4H): the latter direction is parallel to the very strong metamorphic fabric of the NMZ in this part of the area.

Area I: This area again lies within the NMZ of the Limpopo Belt and consists of gneissic rocks and deformed mafic sheets metamorphosed to granulite facies.

On Landsat imagery, a long though weak, NNE lineament is seen trending NNE through the centre of the area; a few short northwesterly lineaments also occur. By contrast, a very high density of lineaments is evident on aerial photographs (Figures 2I and 4I). The principal direction here is between 60° and 80°, corresponding to the main structural trend and the direction of mineralogical banding and parallel fractures seen in many outcrops. Elongated bornhardts along this trend similarly reflect the structural/mineralogical control of erosion. Subsidiary fracture directions trend northwesterly. The distribution of fracture swarms on Figure 2I indicates the presence of distinct NNW, NW and WNW sets: closed, planar, vertical joints along these different directions are common in outcrop. The NNE satellite lineament is only weakly seen on

photographs but is again represented as closed, vertical fractures in outcrops near to where it occurs.

Area J: Area J occupies a similar geological position to area I and consists of strongly banded granulitic gneisses and folded mafic sheets. Complex styles of folding are evident but closures and structural trends are mainly to the ENE.

Several long NNE lineaments are present on Landsat imagery one of which, the probable extension of the Popoteke Fault system, shows apparent sinistral displacement. In the west, two irregular NNW lineaments appear to be extensions of the Sebanga Poort dyke. In the NW corner a broad zone of intense ENE stretching is apparent on the imagery and is also shown on the geological map. A few northwesterly lineaments also occur.

The main NNE and NNW satellite lineaments are seen also on aerial photographs together with other fractures along these trends (Figure 2J). At outcrop, they are manifested as closed, vertical joints: some of the NNE-trending ones are quartz-filled. The main peak on the rose diagram (Figure 4J) is centred at about 70°: once again, this correlates with the average structural trend of the Limpopo Belt and with fractures and erosion along mineral foliation measured at outcrop. However, complex folding produces local variations in the trend of mineral foliation. Other fracture traces seen on the photographs trend between WNW and NW; once again, these correspond to closed, vertical joints on outcrops.

Area K: The rocks of area K are older gneisses, forming poorly exposed, low-relief areas, and younger granites of the Zimbabwe Granite and outlying stocks forming some larger bornhardt masses.

Satellite imagery shows few large fractures in this area, the main ones trending NNW. The photolineament plot (Figure 2K) and rose diagram (Figure 4K) show two, or possibly three, main fracture directions: 70°, 330° and 295°. Both the principal ENE direction and the subsidiary NNW direction are surprisingly well expressed given the limited outcrop, and form an almost rectilinear pattern of drainages. Outcrops of granite and gneiss show the usual pattern of ENE foliation-related fractures (responsible for the elongate form of many outcrops) and cross-cutting northwesterly joints, some quartz-filled but showing little or no indication of movement.

Area L: This area extends over the southwestern tip of the Masvino greenstone belt, a strip of older gneisses in the west, and porphritic granites and part of the Zimbabwe Granite batholith to the east and south. The greenstones form high relief, wooded terrain. Over the granitic area bornhardts are separated by intervening areas of fairly thick regolith (e.g. near Charumbira School).

The frequency of observed fractures is strongly correlated to lithology, few lineaments being recorded within the greenstones on either imagery or photography. Landsat imagery shows several large lineaments mainly within the porphyritic granite and Zimbabwe Granite. Most of these trend NW and NNW (apparently belonging to two different sets), but a long NE lineament is present along the southeast margin of the greenstone belt.

Numerous short lineaments are seen on aerial photographs (Figure 2L), again occurring predominantly within the granites and gneisses, which show concentrations of directions towards the ENE (60°-80°), NW (315°) and WNW (295°). Evidence from outcrops again suggests that the ENE direction corresponds to erosion and fracturing along mineral foliation, but other fracture directions show only moderate correlation with the

directions of nearby photolineaments. However, the predominant trend of fractures is northwesterly. Outcrops of porphyritic granite appear more massive: at one site, quartz-filled veins striking NNW were noted.

Area M: This area is shown on the 1:1,000,000 geological map as consisting of younger granite in the north and older gneiss together with small bodies of ultramafic rocks in the southwest corner. Topography is subdued with low hills separated by large expanses of regolith. Basic gneiss appears to be the most common rock type in outcrop.

The only structures seen on Landsat imagery are a few NNW-trending lineaments. The photolineament plot (Figure 2M) indicates a scattering of generally short fracture traces, some arranged in swarms suggesting more extensive stuctures, notably along NW, NNW and N directions. The rose diagram (Figure 4M) indicates directions in the range 280°-310° to be dominant: most of these fractures are quite short and scattered across the area. Similarly, a peak at about 70° is thought to represent isolated foliation-related fractures. Measurements at outcrop indicated concentrations of joints between NW and NNW and towards the NE. Quartz-filled fractures were recognised among both sets. Once again, the correlation between measured fracture directions and nearby lineaments is not simple: in general, the main local lineament directions are represented at outcrop level but there is not necessarily a simple correlation in relative intensity of development.

Area N: This area is mapped as younger granite on the 1:1,000,000 geological map. Its appearance on imagery indicates it to have extensive regolith cover. It was not visited.

The only stuctures evident on Landsat imagery are a few NNW-trending lineaments and still fewer trending NE. The area is situated, however, between important NW trending faults. By contrast, numerous fractures are apparent at the scale of aerial photographs (Figure 2N) with important concentrations towards the ENE, NE and NW, although every sector of the rose diagram plot (Figure 4N) is represented. There is some suggestion on Figure 2N that swarms of aligned fractures form larger structures: these trend NE, N and NW.

3.2 Summary & discussion

Fracture studies in the Masvingo area suffer from the limitation that outcrops are almost certainly unrepresentative of the rocks underlying regolith where many of the larger lineaments, detected by remote sensing, occur. Bornhardts and low domes represent unfractured kernels (or corestones) between major fractures. Such granite domes are either massive or possess widely spaced fractures (mostly joints) whose directions show only a general correlation with the directions of lineaments identified by remote sensing.

Two main classes of steep fracture occur: closed planar joints along or across the mineral foliation, and narrow quartz-filled fractures (joints and occasional faults). The filled fractures are less common but tend to occur along NNE, NNW and NW directions and often correlate with major lineament directions: they are considered to represent ancient fractures. Closed joints on the other hand are interpreted as young features formed through the release of locked-in palaeostresses during uplift and erosional unloading. They evidently relate to several tectonic events. Their limited correlation with major fractures suggests that they may have developed in response to residual stresses resulting from movements along the main faults.

Although shallow-dipping or horizontal fractures are difficult to detect by remote sensing, sheeting on granite domes and horizontal fractures on 'castle kopjes' are nevertheless common features in the Masvingo region that may have importance in hydrogeology. The exfoliation sheets commonly show a near parallelism to the ground surface and are believed to result from the expansion of rock masses as their confining pressures are released during uplift and erosion. Unloading domes typically form in massive rocks such as granite and occur in all climates (Ollier 1984). Sideways expansion has been observed in many quarries and may be the immediate cause of sheeting where the rock is confined laterally (Folk & Patton 1982). The present-day formation of both vertical and surface-parallel fractures is seen at the Masvingo quarry where the fractures can be seen to develop as quarrying proceeds (Plate 6).

Thus, the role of both steep and flat-lying fractures can be envisaged within the context of an evolving land surface of etchplains and bornhardts along the lines proposed by Thomas (1965). According to this model, zones within the basement cut by major tectonic fractures weather more rapidly than unfractured rock masses which develop as bornhardts during repeated phases of regolith stripping and lowering of the basal surface of weathering (Figure 8). Erosional unloading promotes the release of tectonic palaeostresses to form steep joints while excess expansion results in sheeting. Well-developed horizontal fractures may give rise to castle kopjes.

3.3 Regional analysis

The Landsat-derived dataset (3091 lineaments) shows several well-defined peaks on the length-weighted rose diagram (Figure 5A) providing confirmation that a number of discrete events are

represented as suggested from an earlier qualitative interpretation of the data (Greenbaum 1986a). Despite a spread of values between WNW and NNW, three tectonic events appear to be represented by this sector (sets 1, 3 and 5 below):

(1) 338° (335°-345°): long lineaments and dykes of the Sebanga Poort set cutting through all formations, and shorter lineaments developed locally within the older gneisses and younger granites;

(2) 13° (0°-25°): fractures and dykes of regional extent belonging to the Great "Dyke" set, and other long and short fractures developed within the younger granites and occasionally within other formations;

(3) 303° (295°-310°): numerous short fractures developed mainly in the younger granites;

(4) 78° (60°-80°): infrequent long fractures developed within the younger granites and Limpopo Belt granulites along the regional structural grain;

(5) 284° (275°-290°): widely spaced, long fractures some showing dextral displacement ("Mtshingwe" set).

The combined photolineament dataset represents only the fourteen selected study areas and as such is not directly comparable to the satellite-derived data which is from the entire region. The rose diagram for the aerial photograph data (Figure 5B) shows two main peaks, at 330°-340° and at 60°-80°, and a continuum of directions through all other sectors. The largest peak (ENE) corresponds to fractures parallel to the metamorphic foliation which are much more strongly represented

on aerial photographs than on satellite imagery. The Sebanga Poort trend is also well developed. Other directions (NNE, NW and WNW) are present but poorly defined.

Based on the analysis of lineaments, field observations and published mapping, it is possible to construct a chronology of igneous-tectonic events in the Zimbabwe craton from the late Archaean through to the Phanerozoic (Table 1). Prior to about 3000 Ma the craton had already undergone a complex tectonic evolution involving several ductile events (Coward 1976; 1983; Coward & James 1974; Coward et al. 1976; Wilson 1979). The subsequent history involved a number of major igneous-tectonic events that left their imprint on the geology. The sequence of tectonic events differs in some details from that previously proposed (Greenbaum 1986a).

At least four episodes of major compressive tectonism are recognised, separated by periods of tension and igneous intrusion. Repeated brittle deformation has caused reactivation of some fracture directions: shear fractures have opened under tension and provided ingress to magmas to form dykes, while at other times faults have undergone renewed horizontal movement under a reorientated compressive stress. Consequently, it is difficult on the basis of orientation alone to unequivocally assign a fracture to a particular event or to infer whether it forms part of an open or closed system.

Whereas some of the main fracture sets are extensively developed and exhibit a clearly defined sense of movement (e.g. the dextral strike-slip Mtshingwe Fault set), the corresponding conjugate direction of shearing is often much less prominent and may show little field evidence of movement. This is a common situation where wrench faulting is concerned. However, even where evidence of movement is lacking, the appropriate direction of fracturing is always developed.

Table 1 indicates the inferred orientation of the principal compressive stress during successive periods of tectonism. This shows a steady and progressive shift from NNW-SSE to WNW-ESE. It is summarised in Figure 9.

Table 1: SUMMARY OF MAIN IGNEOUS-TECTONIC EVENTS IN THE ZIMBABWE CRATON

(11) NNW-SSE tension with intrusion of Karroo dyke swarms along a dominantly ENE direction parallel to the structural grain of the Limpopo Mobile Belt.

PHANEROZOIC

PROTEROZOIC

(10) Reactivation of NNE fault (Govarezadza River Fault) to north of Zvishavane with some sinistral movement and downthrow to east. A long, NW-trending fracture along the Runde River in this area may represent a conjugate dextral shear.

(9) WNW-ESE horizontal compression ($\sigma_1 = 285^0$) producing a swarm of ENE faults showing small dextral displacements across the East Dyke: reactivation and movement along ENE Mashaba-Chibi dykes in this area. Elsewhere, possible dextral movement along ENE structural grain and sinistral reactivation of pre-existing NW-SE (originally dextral) shears.

(8) Northeasterly directed tension with intrusion of dolerite dykes along some pre-existing NNW fractures (Sebanga Poort, Busi, Crystal Springs).

(7) NW-SE horizontal compression ($\sigma_1 = 310^0$) producing cratonwide NNW fracturing. Developed as widely spaced very long fractures (individually up to 480 km) and numerous shorter fractures. Landsat interpretation indicates small sinistral displacements (e.g. across Great "Dyke"). Abundant WNW fractures may represent conjugate (dextral) shears.

(6) NNW-SSE horizontal compression ($\sigma_1 = 330^0$) resulting in cratonwide development of major strike-slip dextral faults. Movement on Mtshingwe Fault of about 3 km (displacement on Great "Dyke" and Umvimeela Dyke) and of 1.5 km on western part of Jenya Fault. Northerly sinistral conjugate shears poorly developed with movement possibly accommodated by reactivation of NNE fracture set. Final relaxation of compression, and intrusion of dolerite along some NW-SE faults (Mtshingwe) and silicification of others faults (Gono, Jenya etc.) and joints.

PROTEROZOIC

ARCHAEAN

(5) Uprise of basic magma in the crust under WNW-ESE tension, perhaps accompanying linear arching of the craton, resulting in graben formation and intrusion of the Great "Dyke" layered complex and satellite systems (Main Swarm, East Dyke, Umvimeela). Silicification of minor NNE fracture set. [2460 $\pm$ 16 Ma].

(4) NNW-SSE horizontal compression ($\sigma_1 = 345^0$) resulting in the cratonwide development of major and minor NNE fractures some showing sinistral displacements, and occasional splay faults (e.g. Sabi Mine shear, Zvishavane; Zenda Fault). Well-developed set of conjugate NW fractures (e.g. Chibi Granite) with possible dextral movement.

(3) Emplacement of the "younger" granites. In SE Zimbabwe the batholiths of the Chilimanzi Suite were injected along an ENE zone parallel to the Limpopo Mobile Belt during NNW compression. Development of ENE flow-layering (mineral foliation) dipping steeply to the SSE. [2700 Ma - 2600 Ma].

(2) 12 km sinistral movement along the eastern arm of the Jenya Fault and dextral movement along conjugate Lochinvar, Kenilworth and Mushandike Faults resulting from NE-SW horizontal compression.

(1) Intrusion of ENE, ESE and concentric dykes into the gneisses of the Mashaba-Chibi area (Mashaba-Chibi swarms). [2970 Ma - 2625 Ma].

4. REMARKS CONCERNING BOREHOLE SITING PROCEDURES

Fieldwork included visits to many boreholes throughout the area. At each location the position of the borehole was identified on the aerial photograph (usually to within 20 m or so) and observations made on structures, topography and apparent logistical constraints. From this it is possible to infer how the site was chosen and to comment on the role and importance of structural considerations in the selection procedure.

Lineaments fall into four main categories which can, with experience, usually be distinguished from each other on 1:25,000 aerial photographs:

- fractures (faults & joints)
- mineral foliation (and related partings)
- dykes & veins (mainly dolerite & quartzite)
- pegmatite veins

It is clear from the boreholes visited that all hydrogeological consultants use photogeological techniques as the fundamental approach in selecting sites for detailed geophysical studies. Considerable importance is placed on lineaments if for no other reason than that they are often the only manifestation of the geology, particularly in regolith-covered areas where the majority of water supplies are required. There is good reason to believe that both fractures and dykes can be of hydrogeological significance in basement areas as zones of permeability and barriers to flow, respectively. (Correlation studies still to be undertaken may provide evidence of the relationship between particular fracture/dyke directions and

borehole yield). It is also apparent that the choice of sites is significantly constrained by socialogical considerations, in particular distance from the user community. The problem of providing a large number of localised supplies means that only a limited scientific effort at each site can be justified (a half day's investigation seems usual). This appears to be a major obstacle in providing high-yielding, long-term supplies. In difficult areas, long-term economy might be better served by siting fewer boreholes in more favorable locations (if necessary at greater distances) and pumping to several user communities.

To summarise, then, sites appear to be chosen according to the following sequence of priorities:

(1) identify localities within easy access of the user community (e.g. along a path; within 1 km maximum);

(2) identify from aerial photographs all lineaments within these localities;

(3) favour photolineaments occupying topographic lows, preferably having a large catchment area (if no lineaments are apparent, select base-of-slope locations with large catchment);

(4) select geophysical traverses according to relationship between lineament and topography - favoured are dykes trending across the slope or fractures in base-of-slope situations outside of the zone of potential surface flooding;

(5) finally, use geophysical results to refine drill site position.

Given the constraints, traverses selected for geophysical surveys are in many instances likely to be compromises. Within the time normally alloted, the geophysical survey can be expected to do little more identify a generally favourable position along one or other already chosen traverse. Moreover, in view of the limitations of commonly used geophysical techniques one must question the extent to which such surveys really help in precisely defining a site, especially since many lineaments can be accurately located from the aerial photograph alone. Often the main problem lies not in being able to locate the lineament but in deciding where along it one can practically site a borehole. In cultivated areas where natural patterns of vegetation have been destroyed by clearing, few lineaments are seen and the better ones usually occur along stream channels. In such cases the lineament cannot be drilled directly with a vertical hole and the usual solution is either to drill near the base of slope as close to the lineament as possible or at the valley head along the projected extension of the fracture. (Here geophysics has a more positive role in confirming the continuation of the structure). One expected result of the present study is a better understanding of how geophysical measurements can be used to supplement information on the nature of the fracture, in particular its width. My observations suggest that many steep fractures are quite narrow - perhaps a metre, more or less. If this is generally the case, one must question whether off-fracture locations have any validity.

5. FUTURE WORK

Notwithstanding the conclusions presented above, there remains some uncertainty as to the precise significance of the minor joint and fault patterns measured at outcrop and their relationship to inferred major fractures (lineaments). Some further analysis of the data already collected is planned as well as re-visits to field stations.

As part of the forthcoming drilling programme it would be valuable to obtain a comparison between the fracturing of basement rocks in outcrop and underlying regolith. It has been suggested above that the exposed basement is unrepresentative of buried areas, but this requires verification. The other general objective of the drilling programme from a stucture viewpoint is to provide information on the physical nature of fractures and dykes. It is strongly recommended that some inclined drilling is done, both as a research technique to obtain detailed information across a dyke or fracture, and as a test of any improved yield resulting from intersecting a greater width of the fracture/dyke plus any satellite zones of fracturing. Pump performance in inclined holes could also be assessed.

Correlation of lineament locations, orientations and lengths with borehole parameters (especially yield) remains to be undertaken in collaboration with others during the final phase of the project. As part of this work, the lineament density plots (Figures 3A to N) - here included but not discussed - will be utilised. Lineament plots showing dykes as well as fractures will also be generated for this purpose. Finally, as noted earlier, some re-interpretation of aerial photographs around boreholes showing no apparent relationship to structures will be undertaken.

6. REFERENCES

COWARD, M.P. 1976. Archaean deformation patterns in southern Africa. Phil. Trans. R. Soc. Lond., A, 283, 313-331.

COWARD, M.P. 1983. Some thoughts on the tectonics of the Limpopo Belt. Spec. Publ. geol. Soc. S. Afr., 8, 175-180.

COWARD, M.P. and JAMES, P.R. 1974. The deformation patterns of two Archaean greenstone belts in Rhodesia and Botswana. Precambrian Research, 1, 235-258.

COWARD, M.P., JAMES, P.R. and WRIGHT, L. 1976. Northern margin of the Limpopo mobile belt, southern Africa. Bull. geol. Soc. Amer., 87, 601-611.

FOLK, R.L. and PATTON, E.B. 1982. Buttressed expansion of granite and development of grus in central Texas. Zeit. f. Geomorph., 26, 17-32.

GREENBAUM, D. 1985. Review of remote sensing applications to groundwater exploration in basement and regolith. British Geological Survey, Overseas Directorate report, 85/8, 36 pp.

GREENBAUM, D. 1986a. Tectonic investigation of Masvingo Province, Zimbabwe: preliminary report. British Geological Survey, Overseas Directorate report, MP/86/2/R, 35 pp.

GREENBAUM, D. 1986b. Comments on 1986 field structural investigations in Masvingo Province, Zimbabwe and notes on follow-up geophysical surveys. British Geological Survey, Overseas Directorate report, 16 pp.

OLLIER, C. 1984. Weathering. Geomorphology Texts, 2. Longman, London & New York, 270 pp.

ROBERTSON, I.D.M. 1974. Explanation of the geological map of the country south of Chibi. Short report geol. Surv. Rhodesia, 40 pp.

THOMAS, M.F. 1965. Some aspects of the geomorphology of tors and domes in Nigeria. Zeit. f. Geomorph., 9, 63-81.

WILSON, J.F. 1979. A preliminary reappraisal of the Rhodesian Basement Complex. Spec. Publ. geol. Surv. S. Afr., 5, 1-23.

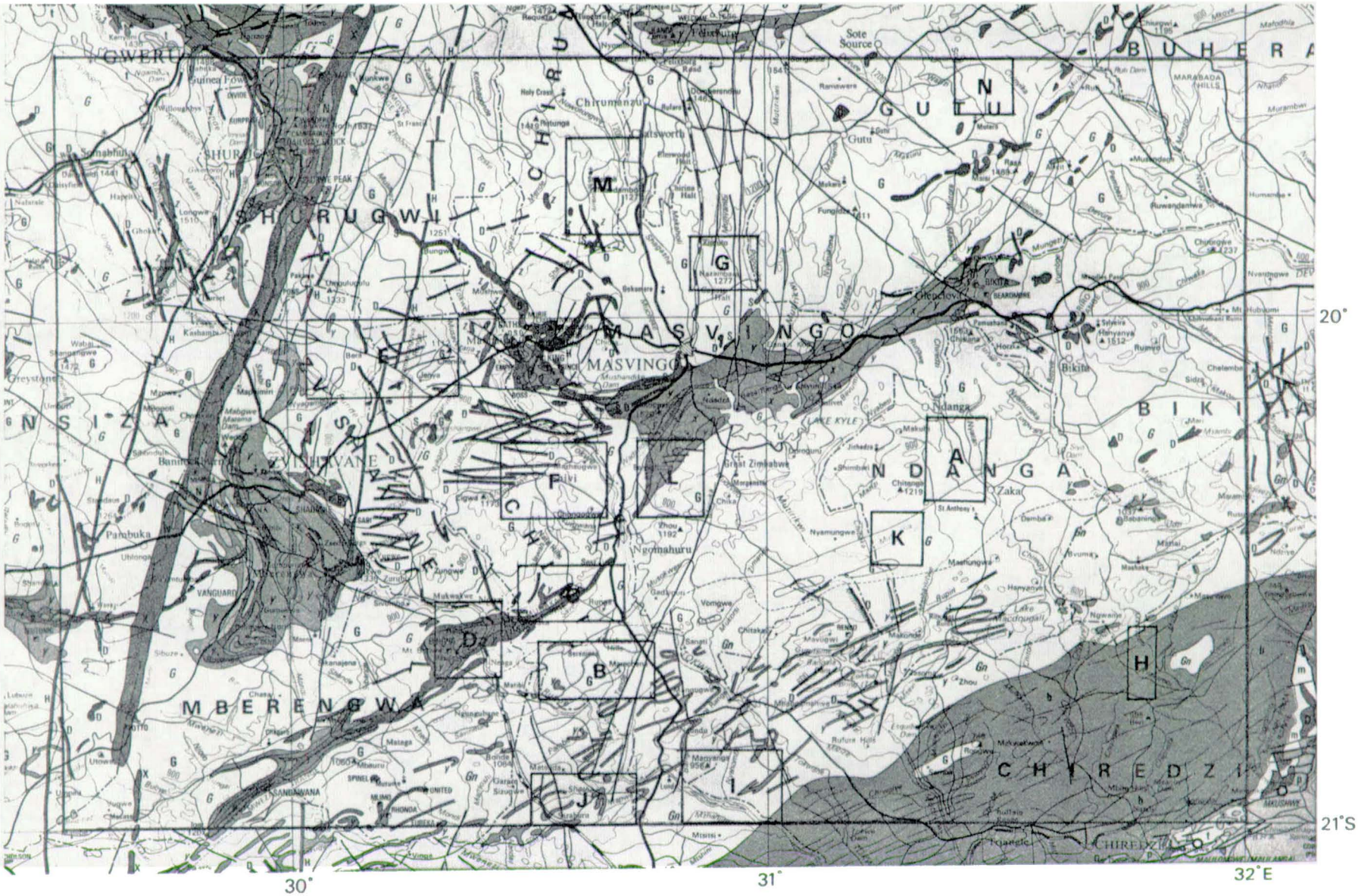

Figure 1: Regional geology and locations of the detailed study areas (A to N).

Figures 2A to N: Computer-generated lineament plots of study areas A to N. Only fracture data is represented except in the case of area E which comprises both fracture and dyke data.

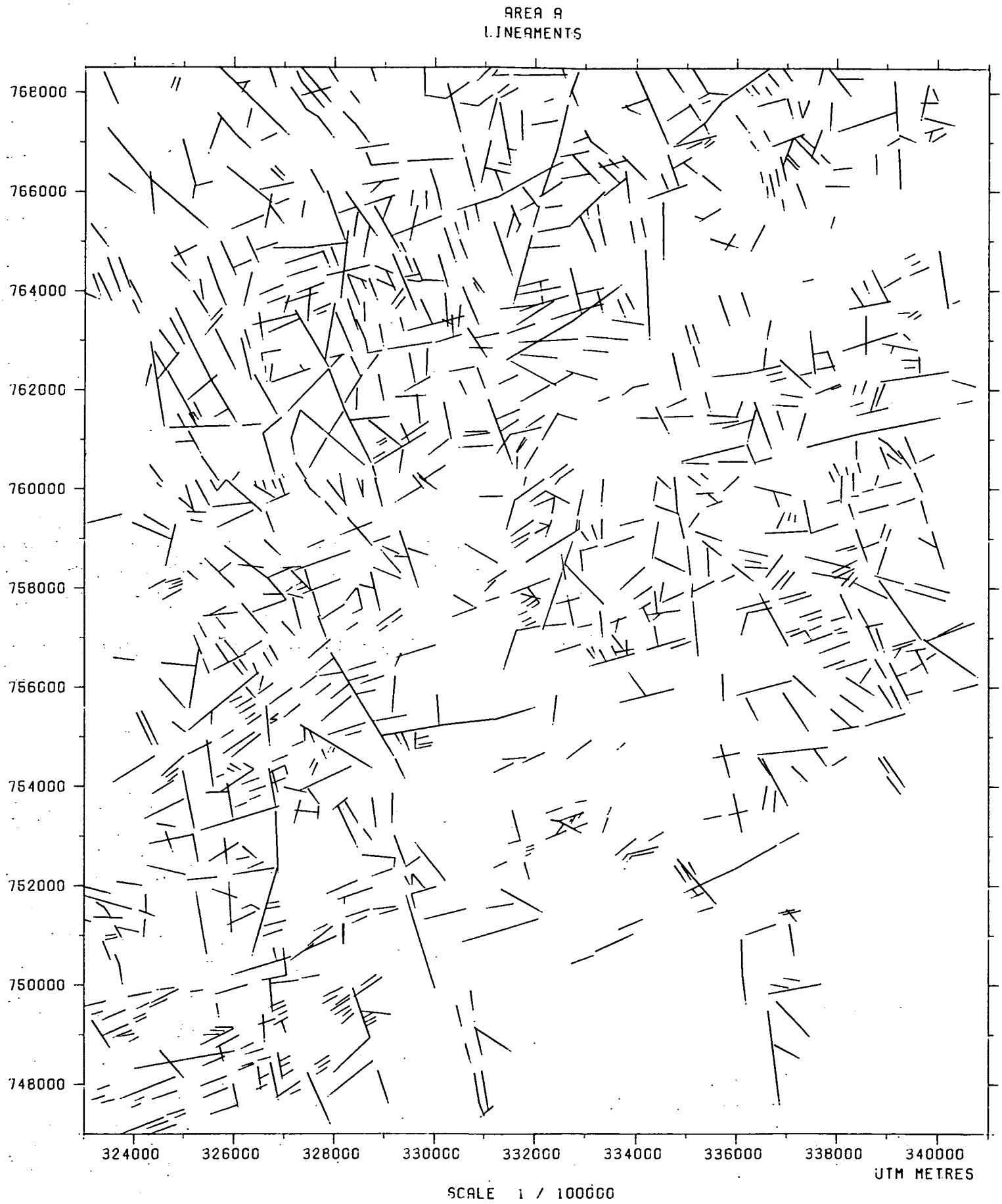
AREA A
LINEAMENTS
768000
766000
764000
762000
760000
758000
756000
754000
752000
750000
748000
324000
326000
328000
330000
332000
334000
336000
338000
340000
UTM METRES
SCALE 1 / 100000

Figure 2A

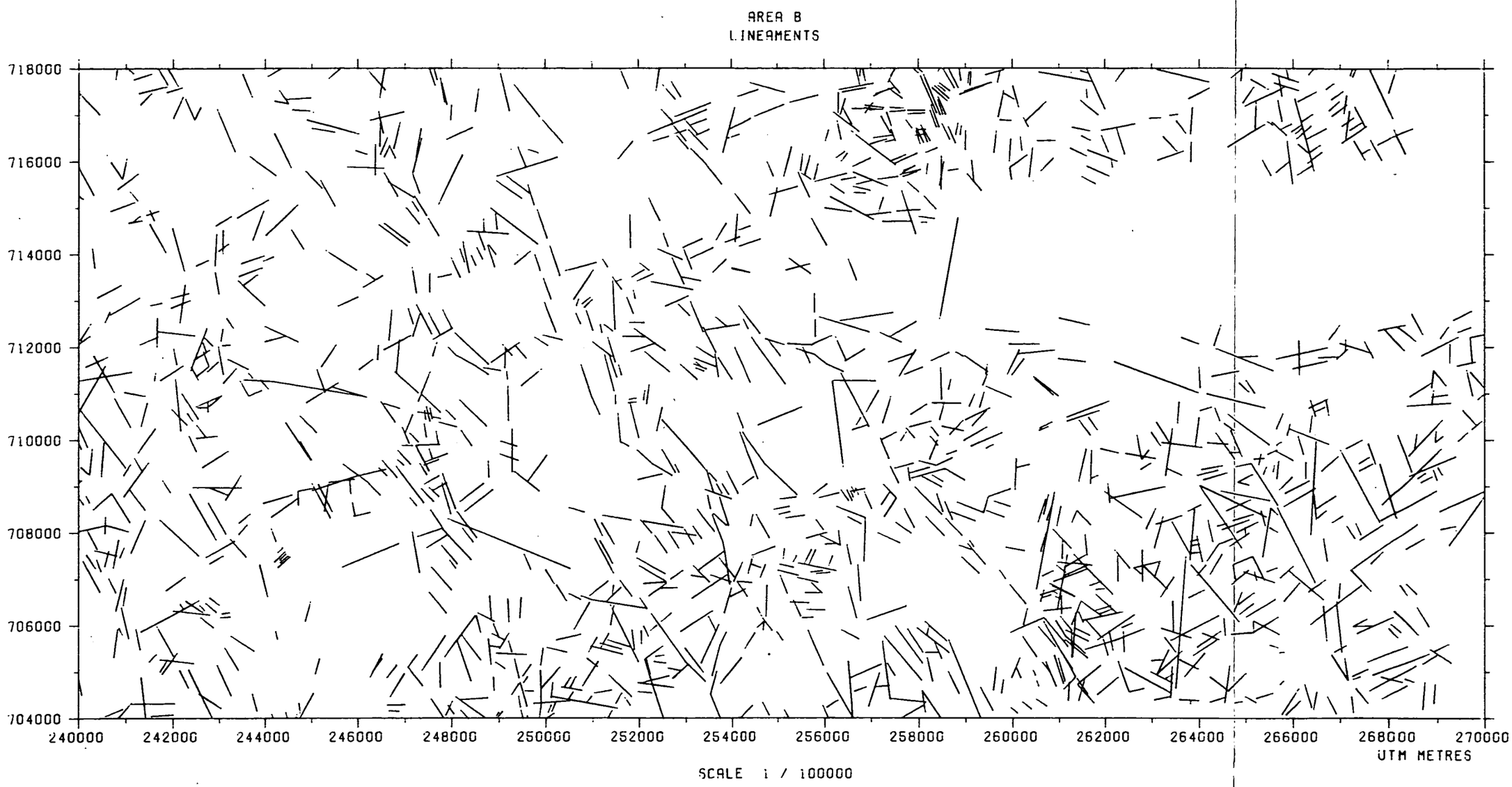
AREA B
LINEAMENTS
718000
716000
714000
712000
710000
708000
706000
704000
240000
242000
244000
246000
248000
250000
252000
254000
256000
258000
260000
262000
264000
266000
268000
270000
UTM METRES
SCALE 1 / 100000

Figure 2B

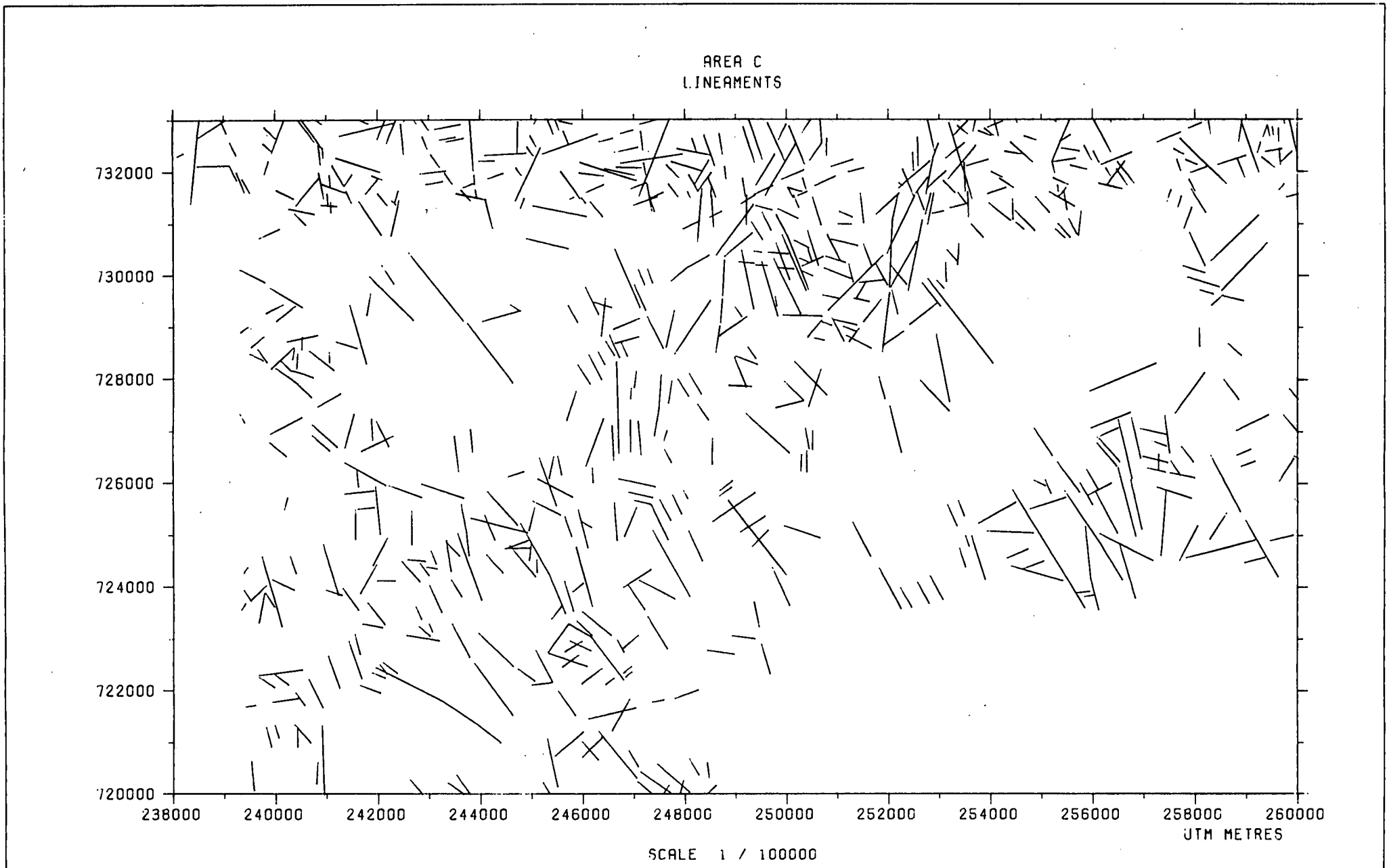
AREA C
LINEAMENTS
732000
730000
728000
726000
724000
722000
720000
238000
240000
242000
244000
246000
248000
250000
252000
254000
256000
258000
260000
UTM METRES
SCALE 1 / 100000

Figure 2C

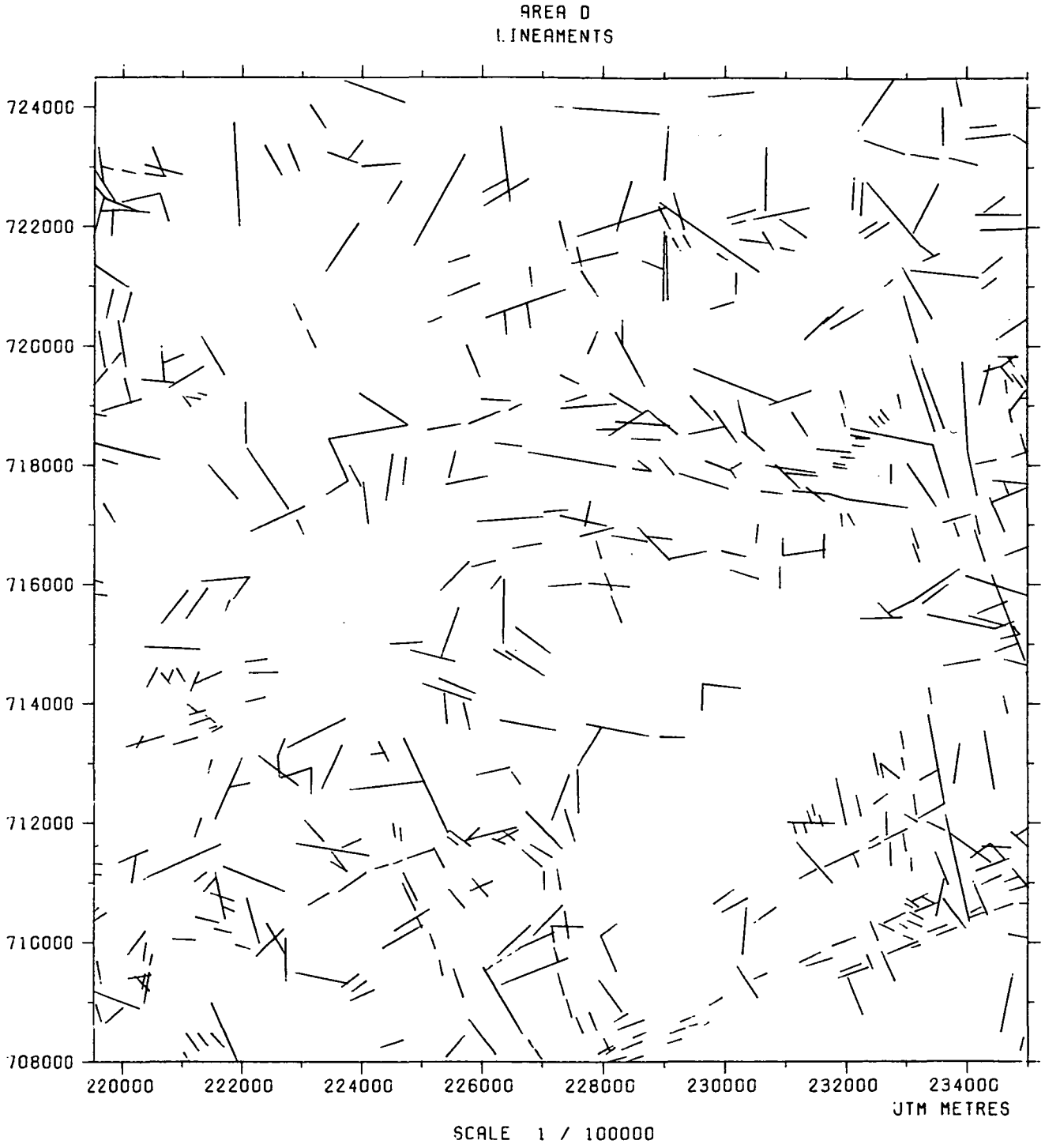
AREA D
LINEAMENTS
724000
722000
720000
718000
716000
714000
712000
710000
708000
220000
222000
224000
226000
228000
230000
232000
234000
UTM METRES
SCALE 1 / 100000

Figure 2D

AREA E
LINEAMENTS

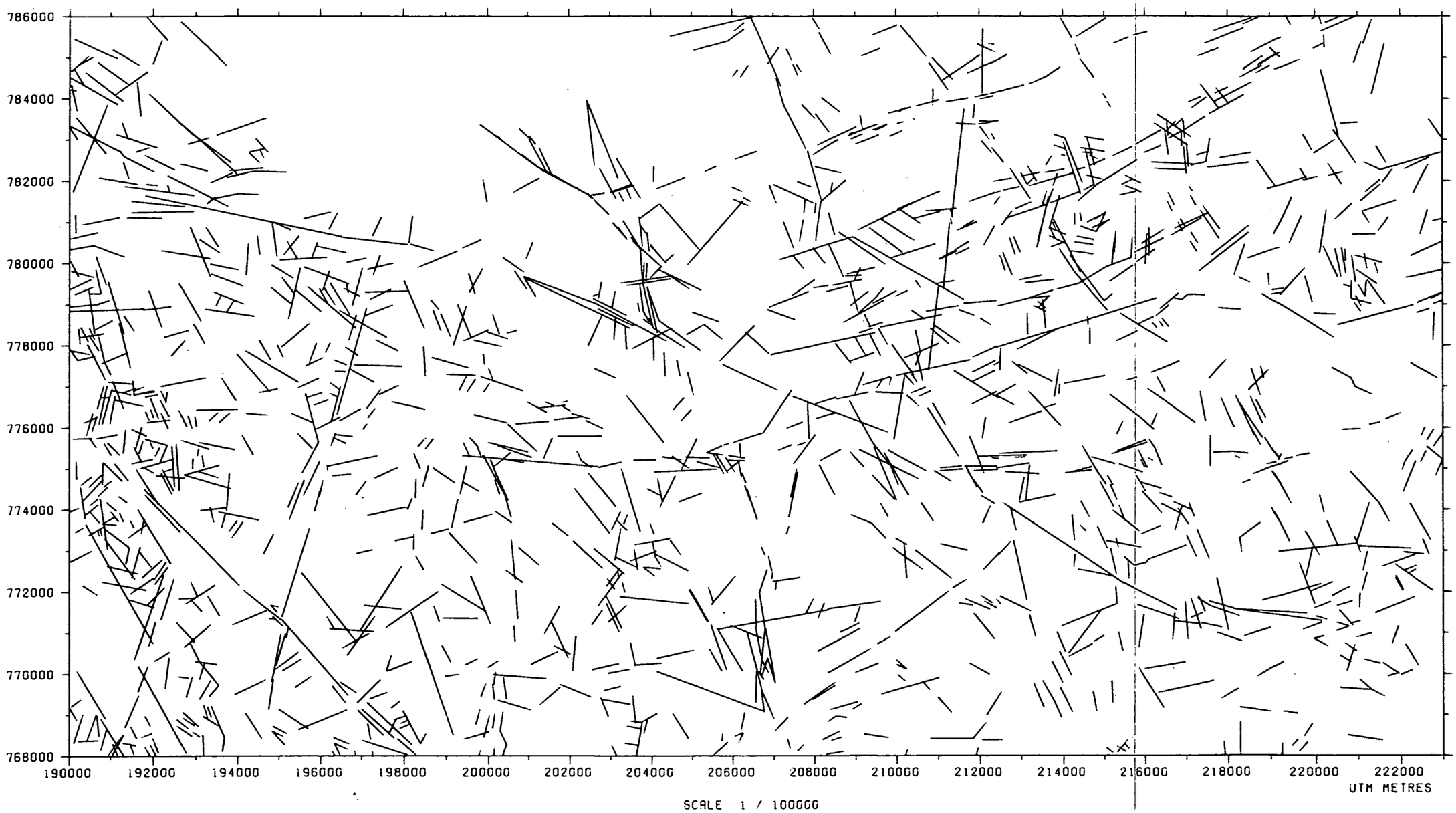

SCALE 1 / 100000

Figure 2E

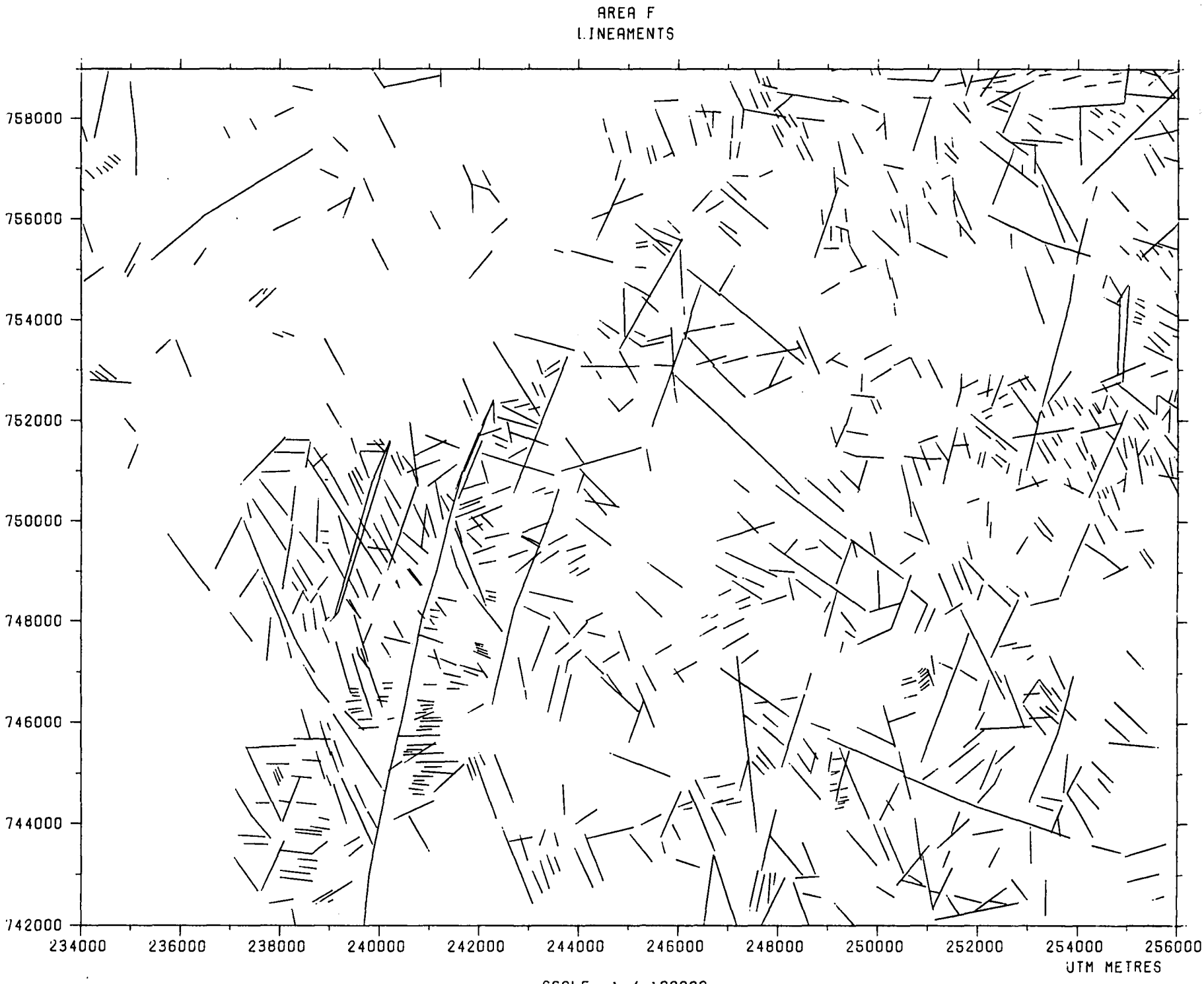
AREA F
LINEAMENTS
758000
756000
754000
752000
750000
748000
746000
744000
742000
234000
236000
238000
240000
242000
244000
246000
248000
250000
252000
254000
256000
UTM METRES
SCALE 1 / 100000

Figure 2F

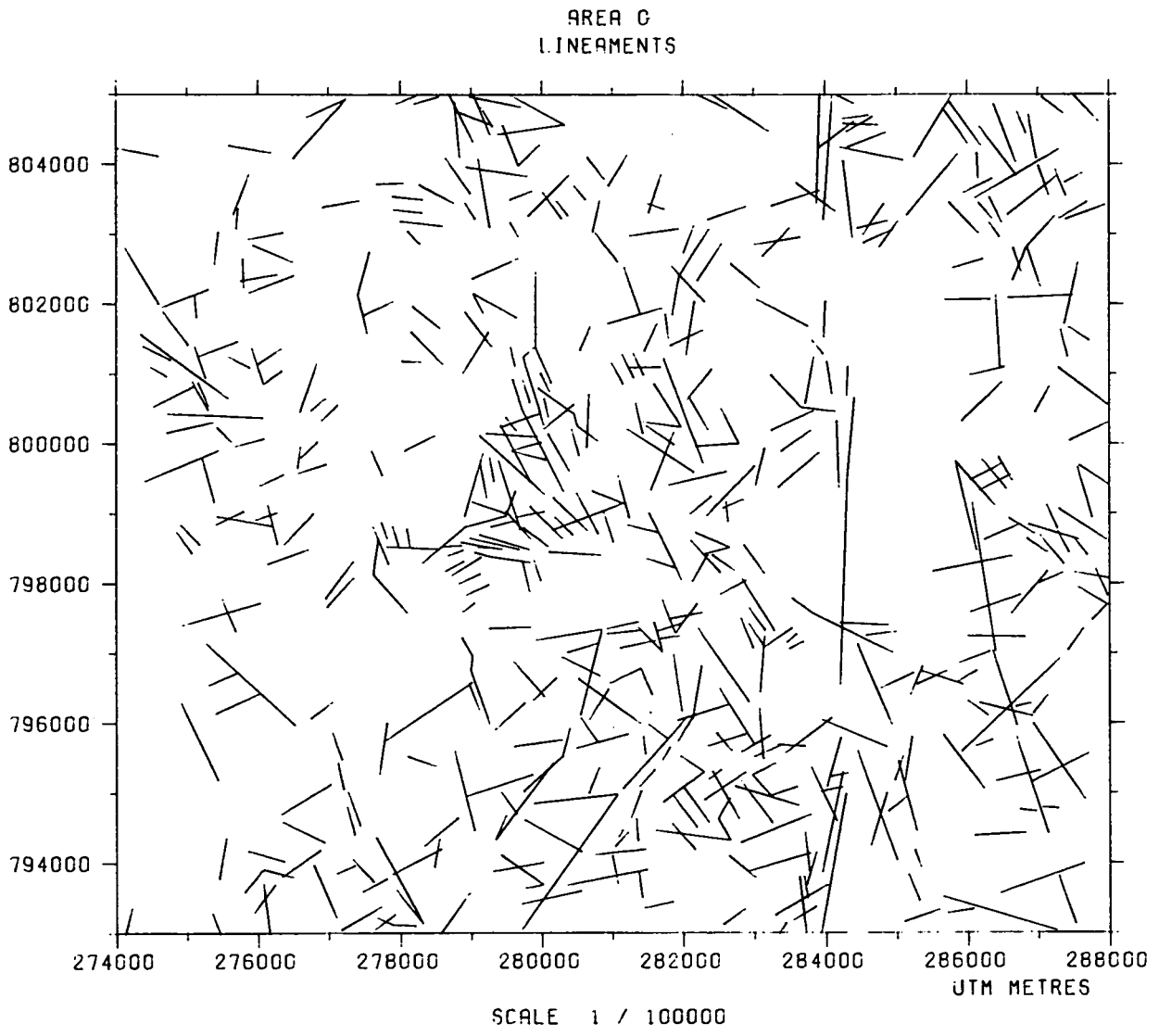
AREA C
LINEAMENTS
804000
802000
800000
798000
796000
794000
274000
276000
278000
280000
282000
284000
286000
288000
UTM METRES
SCALE 1 / 100000

Figure 2G

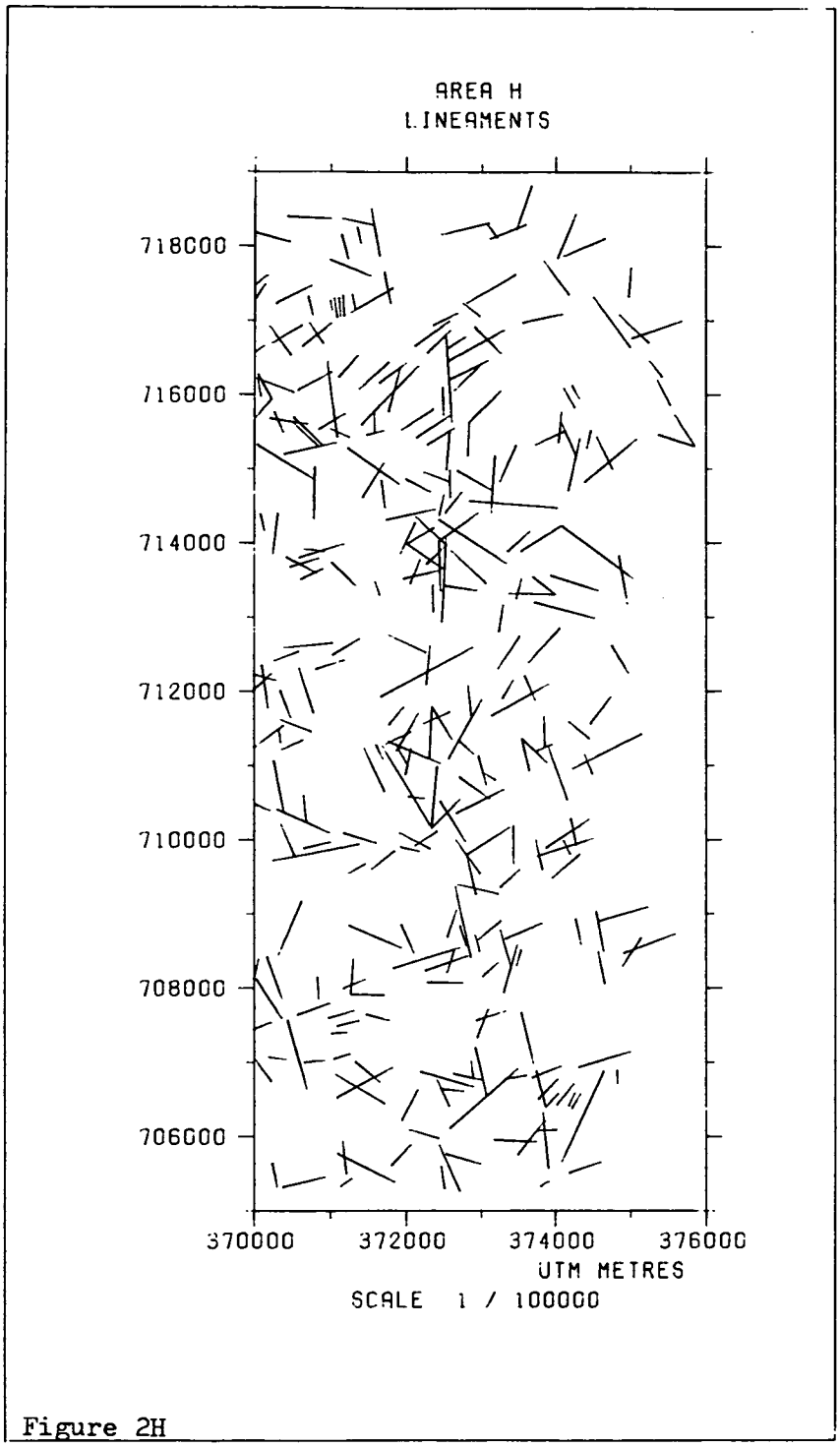
AREA H
LINEAMENTS
718000
716000
714000
712000
710000
708000
706000
370000
372000
374000
376000
UTM METRES
SCALE 1 / 100000

Figure 2H

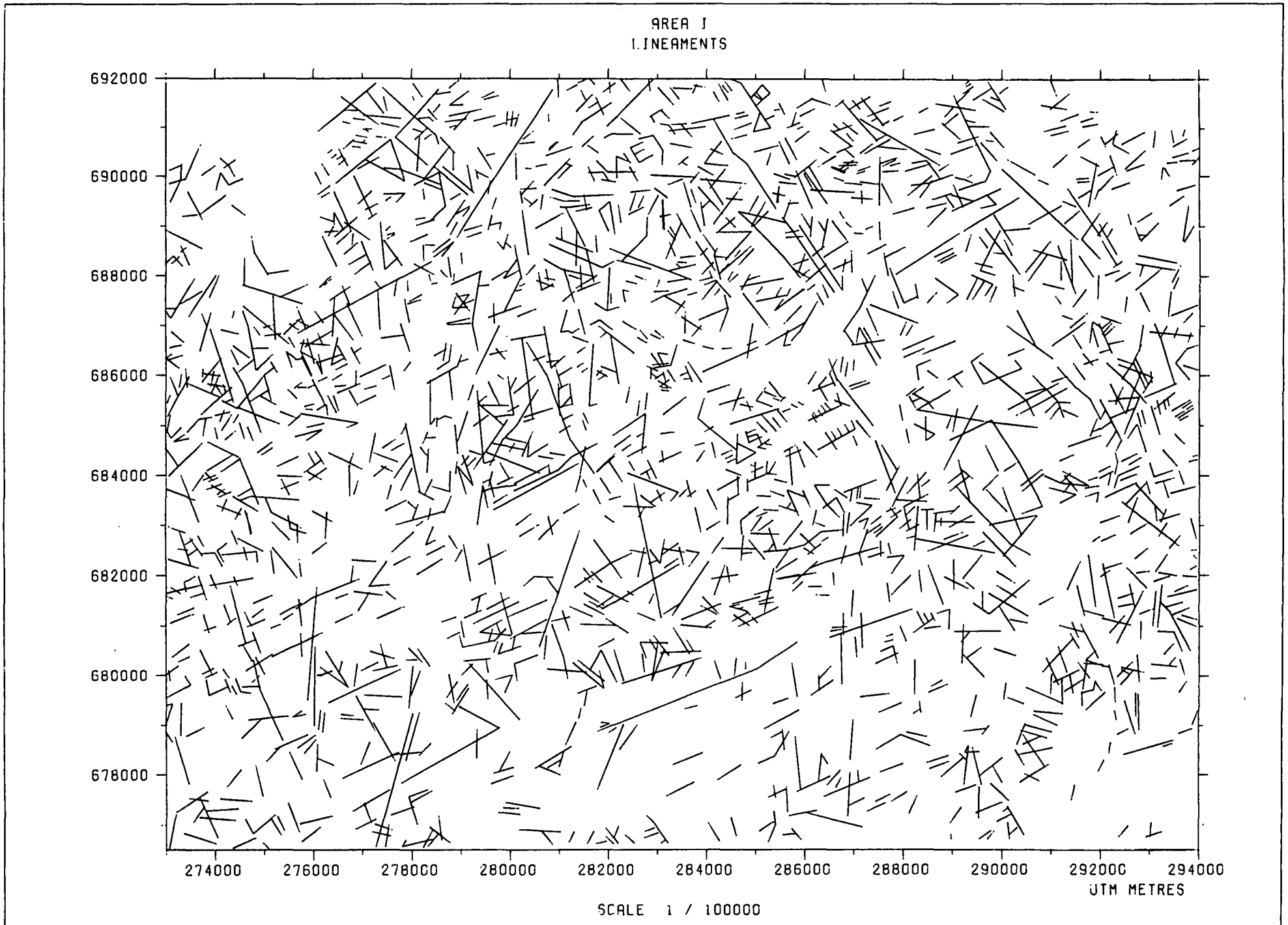
AREA I
LINEAMENTS
692000
690000
688000
686000
684000
682000
680000
678000
274000
276000
278000
280000
282000
284000
286000
288000
290000
292000
294000
UTM METRES
SCALE 1 / 100000

Figure 2I

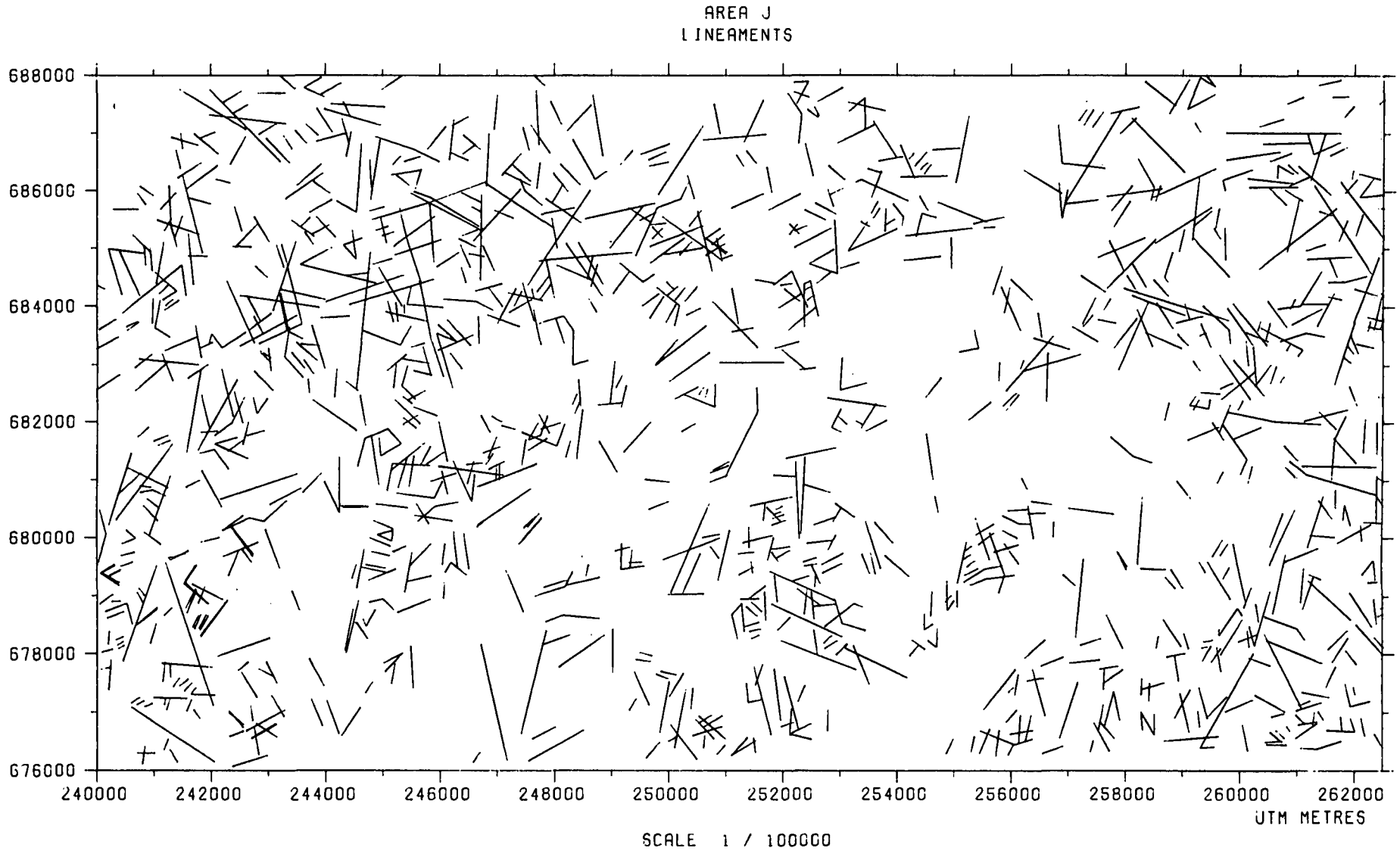
AREA J
LINEAMENTS
688000
686000
684000
682000
680000
678000
676000
240000
242000
244000
246000
248000
250000
252000
254000
256000
258000
260000
262000
UTM METRES
SCALE 1 / 100000

Figure 2J

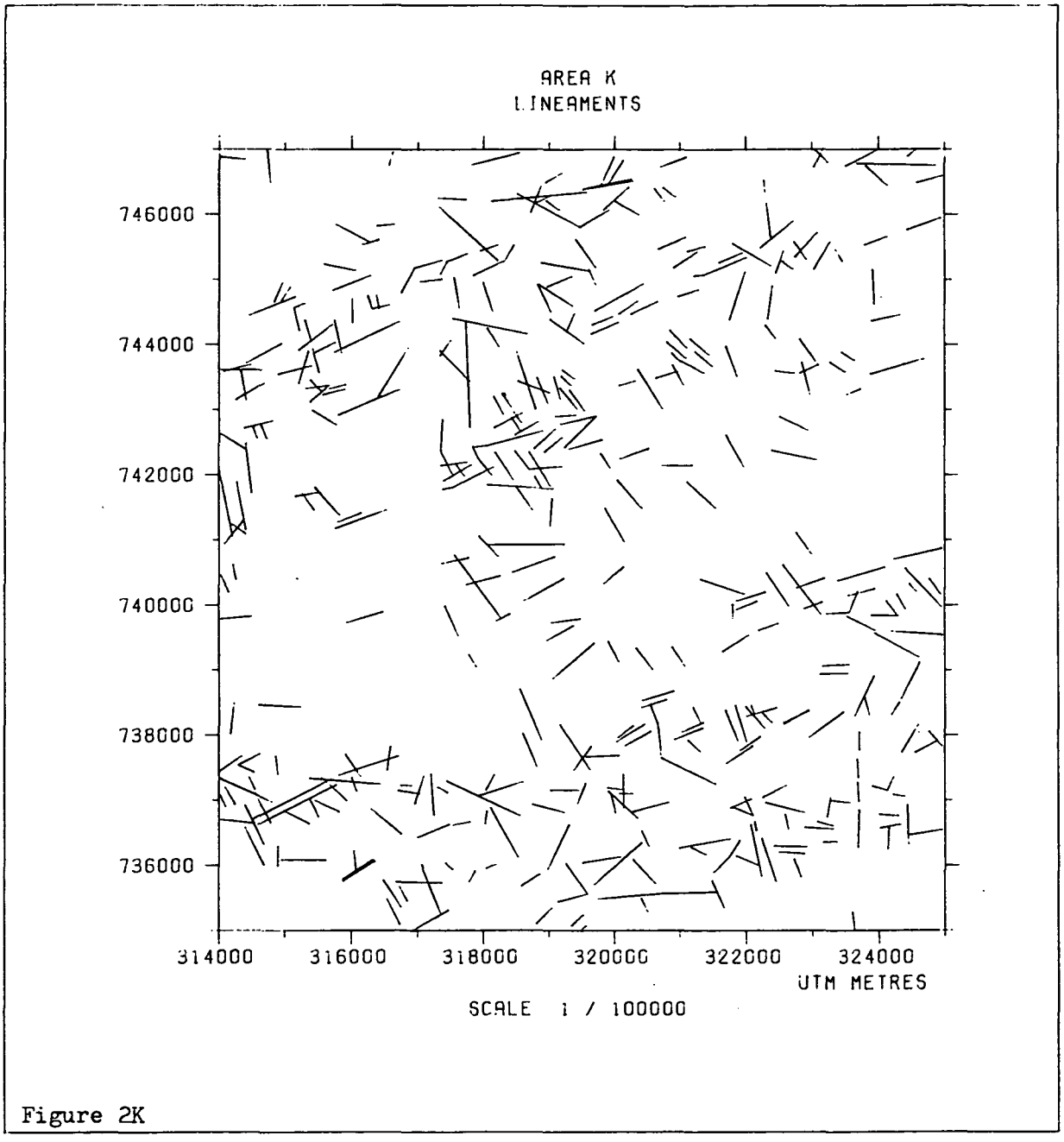
AREA K
LINEAMENTS
746000
744000
742000
740000
738000
736000
314000
316000
318000
320000
322000
324000
UTM METRES
SCALE 1 / 100000

Figure 2K

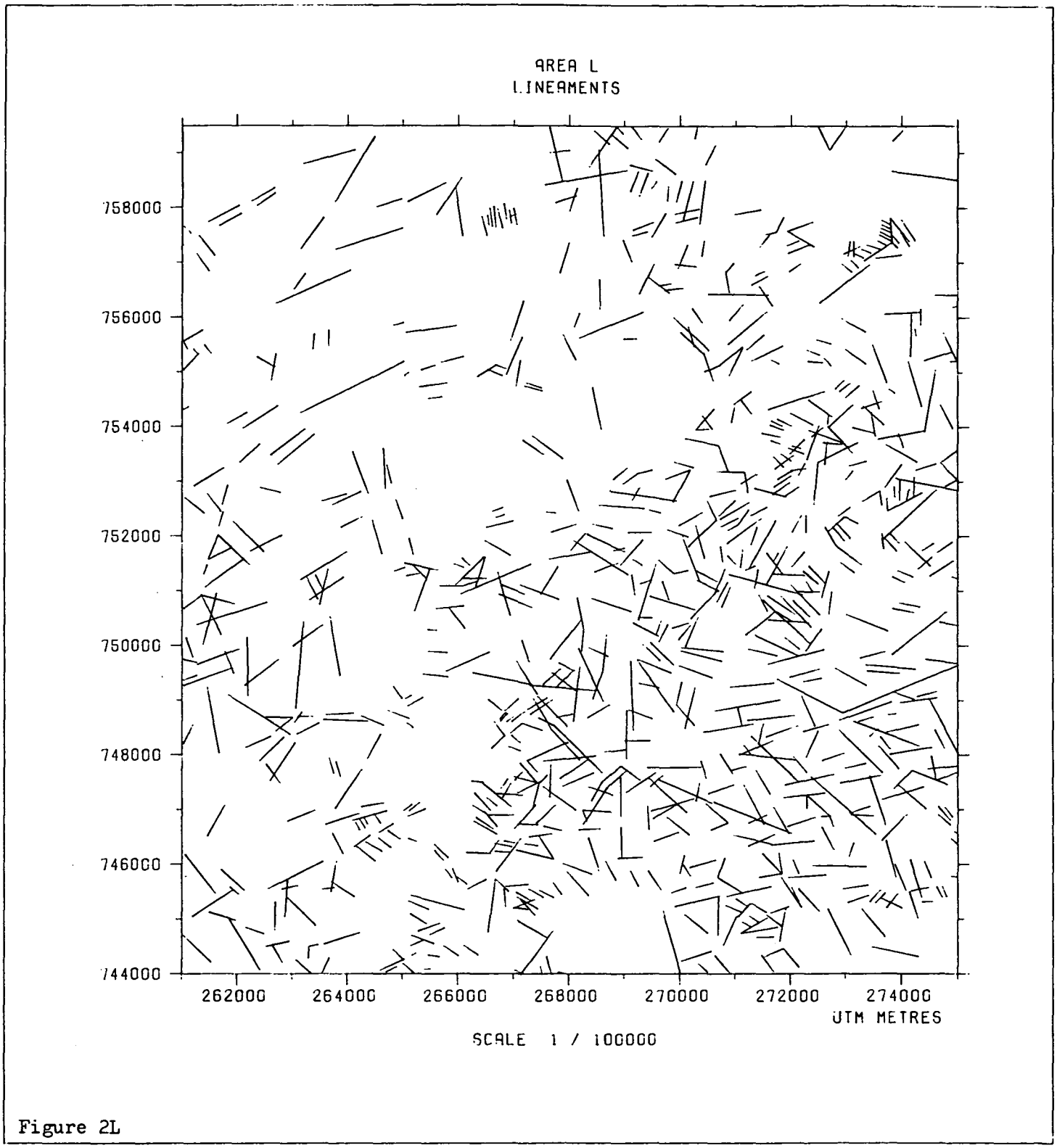
AREA L
LINEAMENTS
758000
756000
754000
752000
750000
748000
746000
744000
262000
264000
266000
268000
270000
272000
274000
UTM METRES
SCALE 1 / 100000

Figure 2L

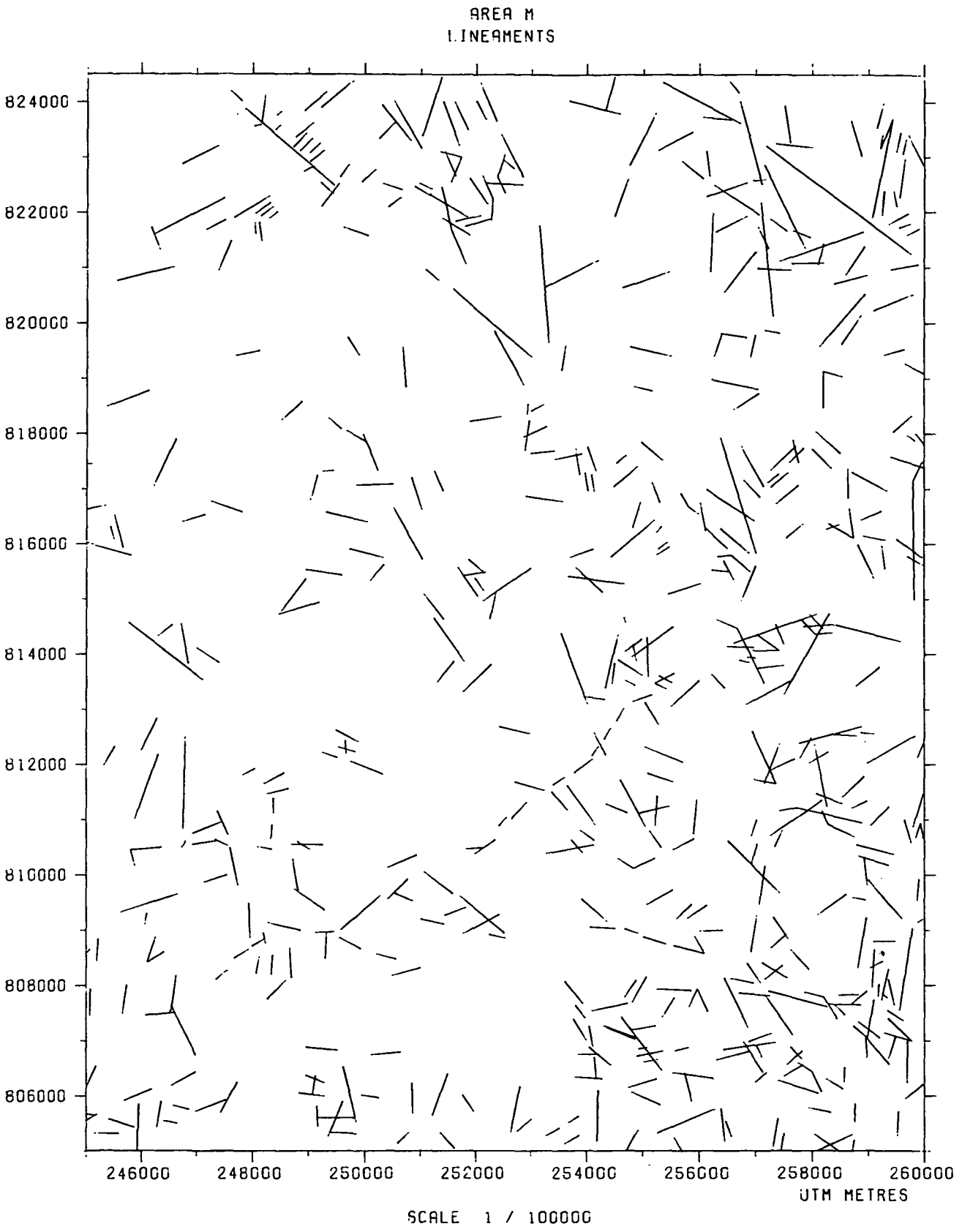
AREA M
LINEAMENTS
824000
822000
820000
818000
816000
814000
812000
810000
808000
806000
246000
248000
250000
252000
254000
256000
258000
260000
UTM METRES
SCALE 1 / 100000

Figure 2M

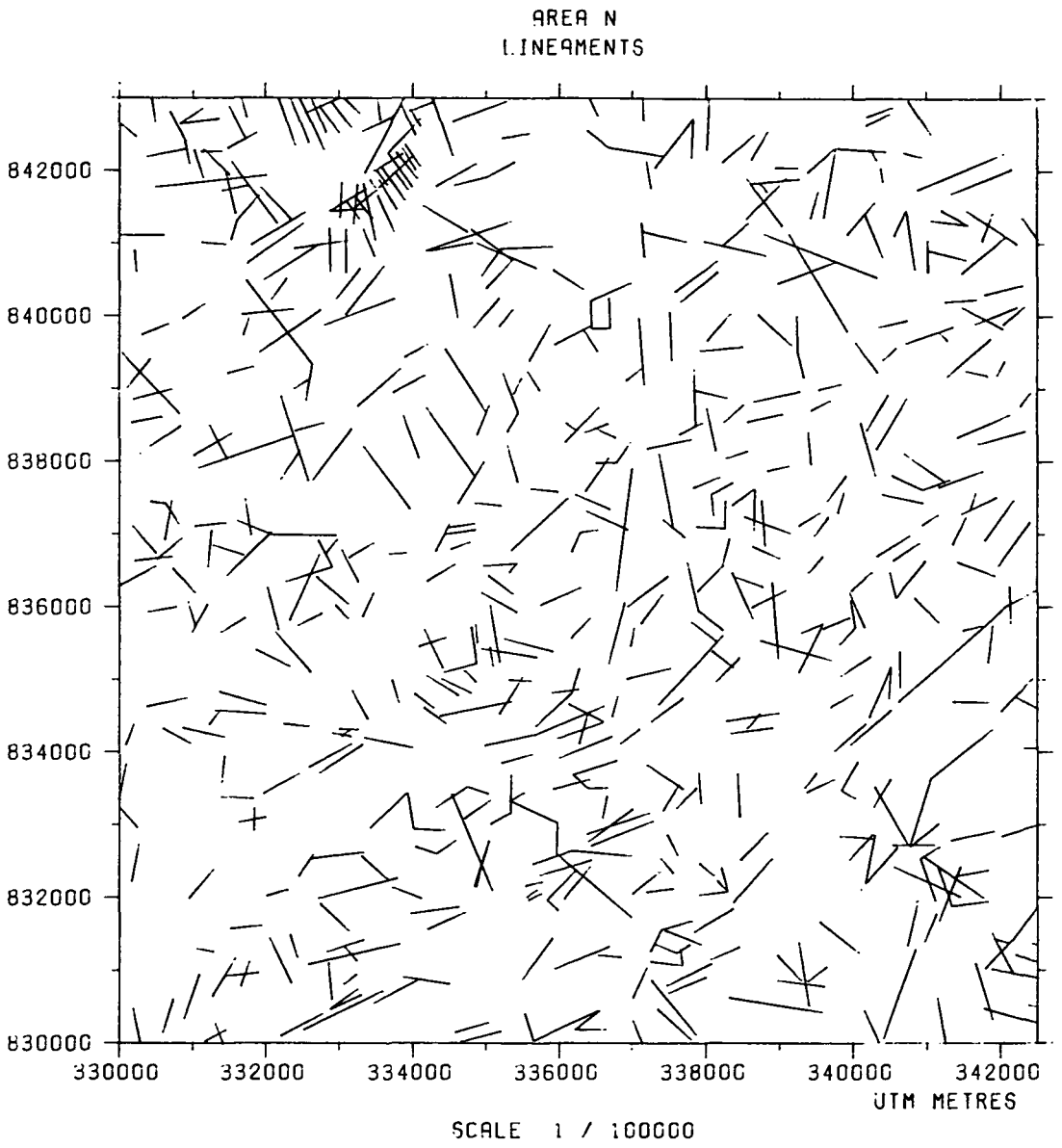
AREA N
LINEAMENTS
842000
840000
838000
836000
834000
832000
830000
330000
332000
334000
336000
338000
340000
342000
UTM METRES
SCALE 1 / 100000

Figure 2N

Figures 3A to N: Computer-generated lineament density plots for study areas A to N, derived from the data illustrated in Figures 2A to N. Lineament density is calculated using a moving-average technique with a 1 km^2 window, and is measured in units of summed-lineament length per km^2.

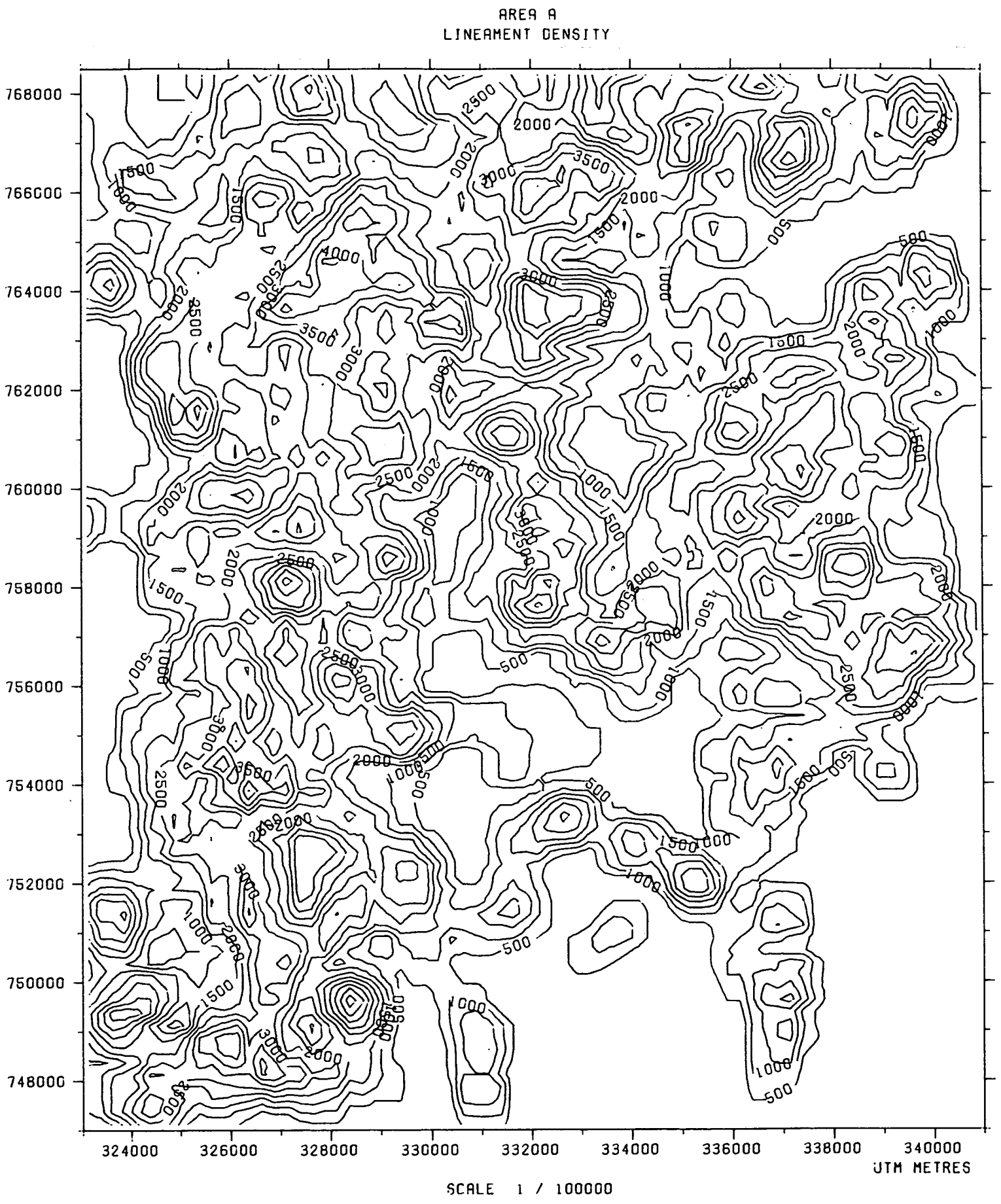
AREA A
LINEAMENT DENSITY
768000
766000
764000
762000
760000
758000
756000
754000
752000
750000
748000
324000
326000
328000
330000
332000
334000
336000
338000
340000
UTM METRES
SCALE 1 / 100000

Figure 3A

AREA B
LINEAMENT DENSITY

718000
716000
714000
712000
710000
708000
706000
704000

240000 242000 244000 246000 248000 250000 252000 254000 256000 258000 260000 262000 264000 266000 268000 270000

UTM METRES

SCALE 1 / 100000

Figure 3B

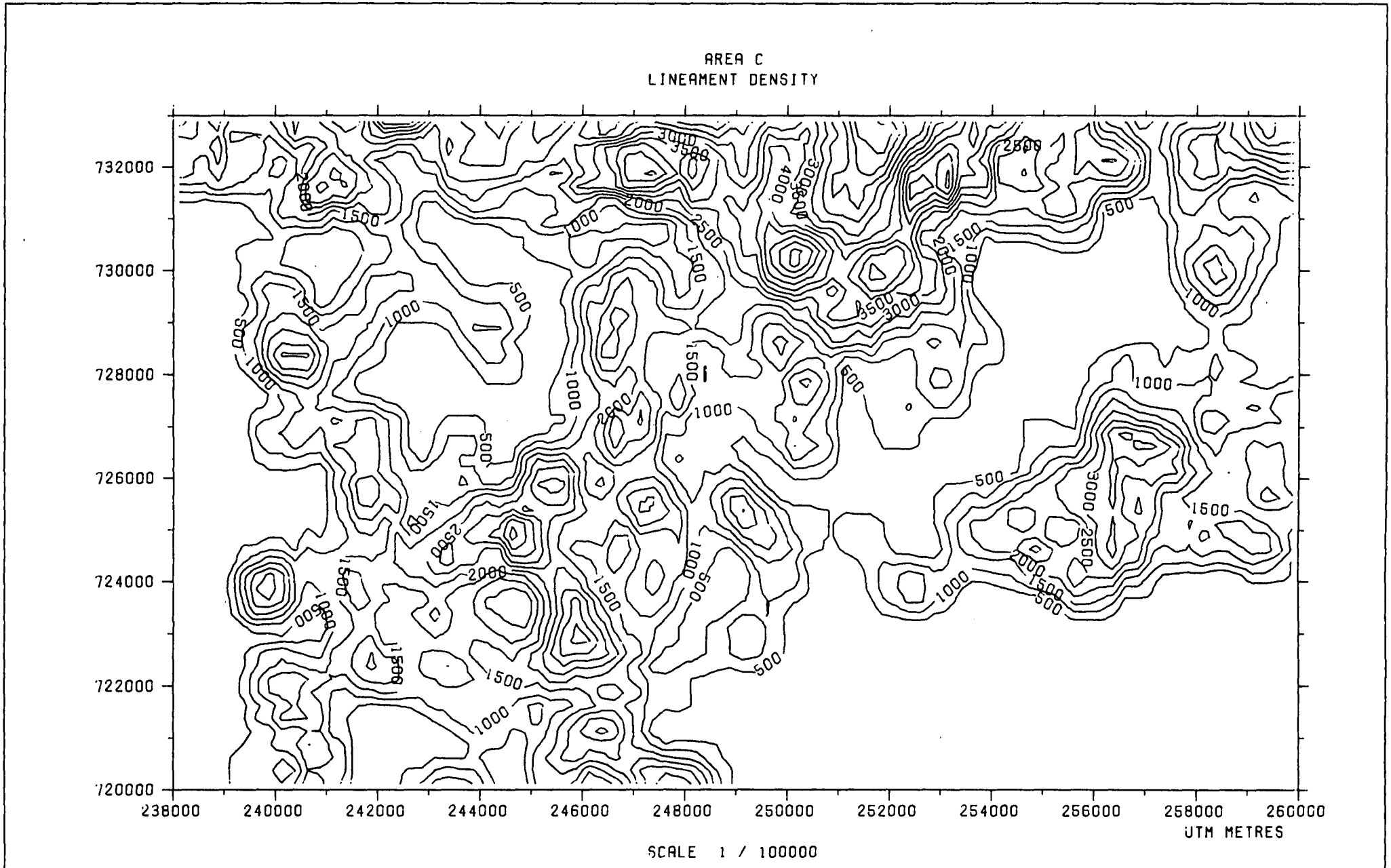
AREA C
LINEAMENT DENSITY
732000
730000
728000
726000
724000
722000
720000
238000
240000
242000
244000
246000
248000
250000
252000
254000
256000
258000
260000
UTM METRES
SCALE 1 / 100000

Figure 3C

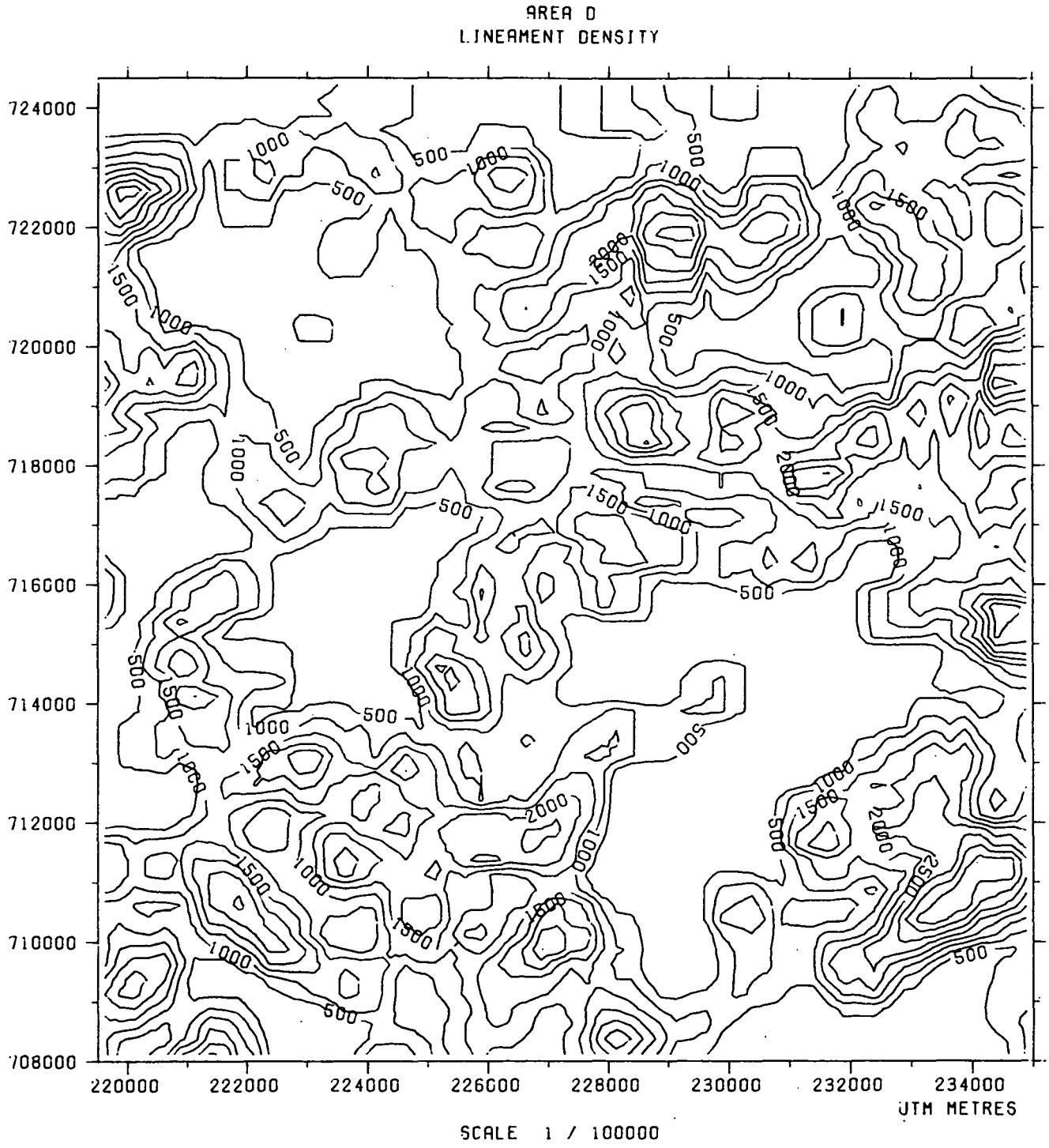
AREA D
LINEAMENT DENSITY
724000
722000
720000
718000
716000
714000
712000
710000
708000
220000
222000
224000
226000
228000
230000
232000
234000
UTM METRES
SCALE 1 / 100000

Figure 3D

AREA E
LINEAMENT DENSITY

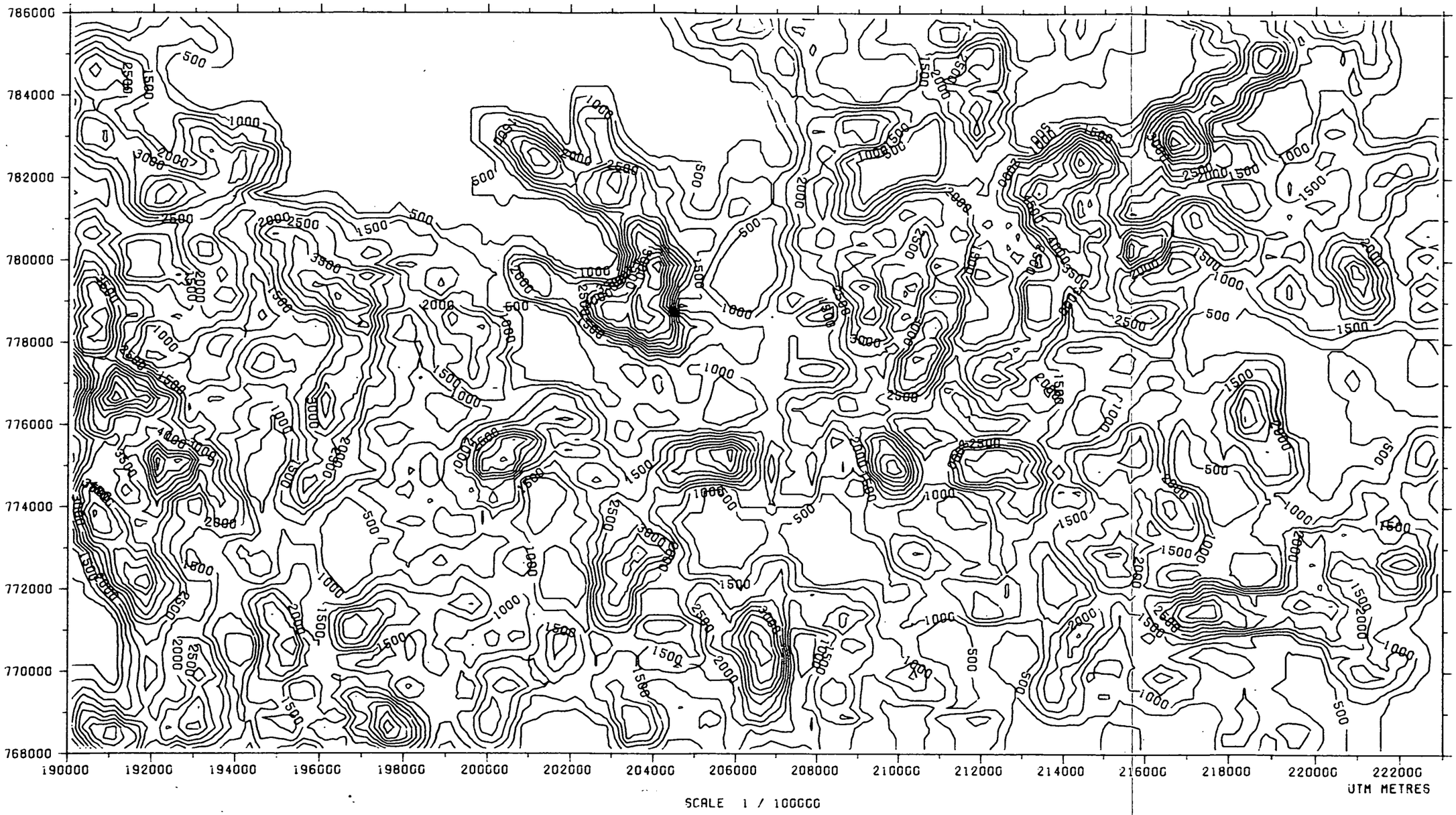

SCALE 1 / 100000

Figure 3E

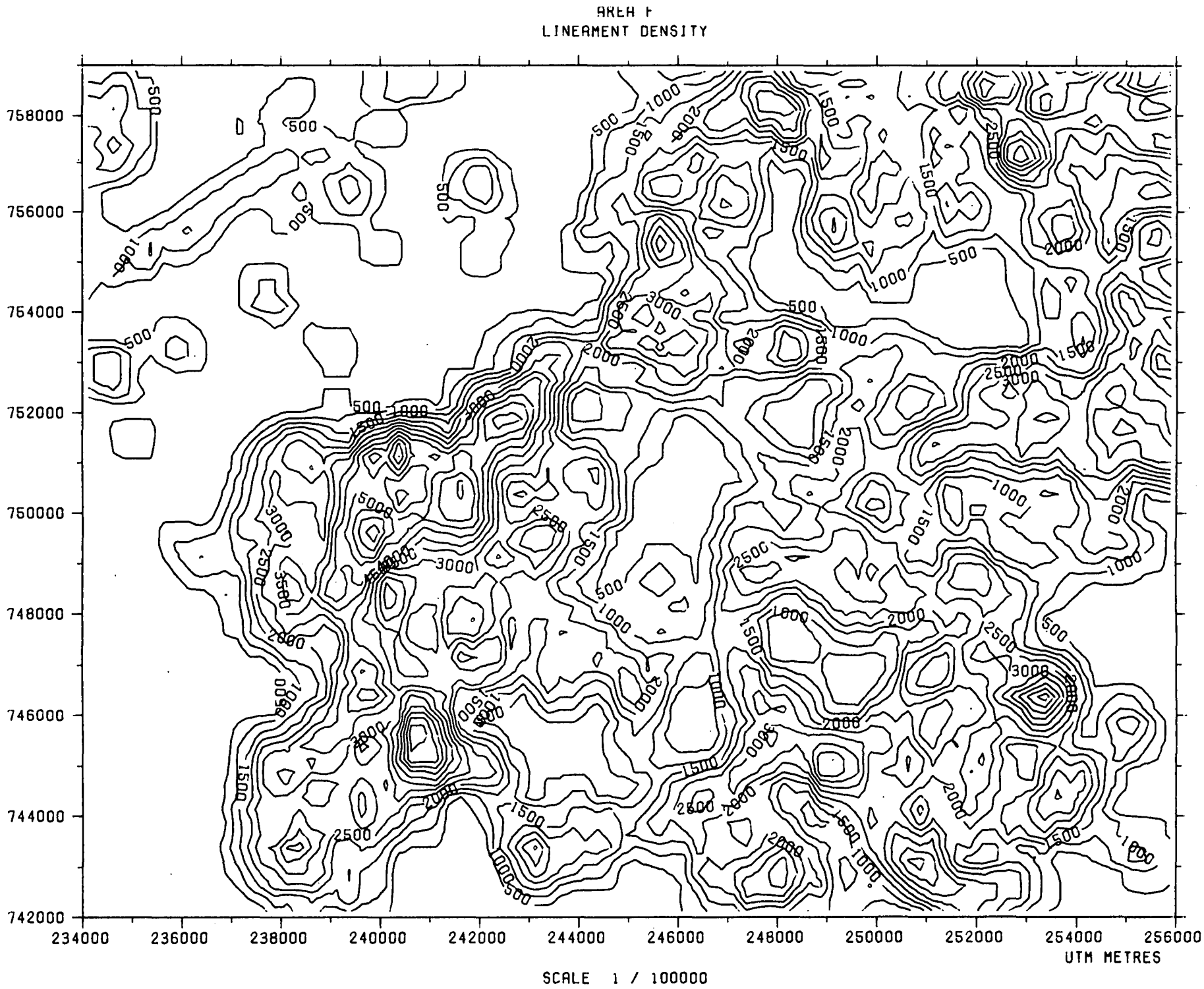
AREA F
LINEAMENT DENSITY
758000
756000
754000
752000
750000
748000
746000
744000
742000
234000
236000
238000
240000
242000
244000
246000
248000
250000
252000
254000
256000
UTM METRES
SCALE 1 / 100000

Figure 3F

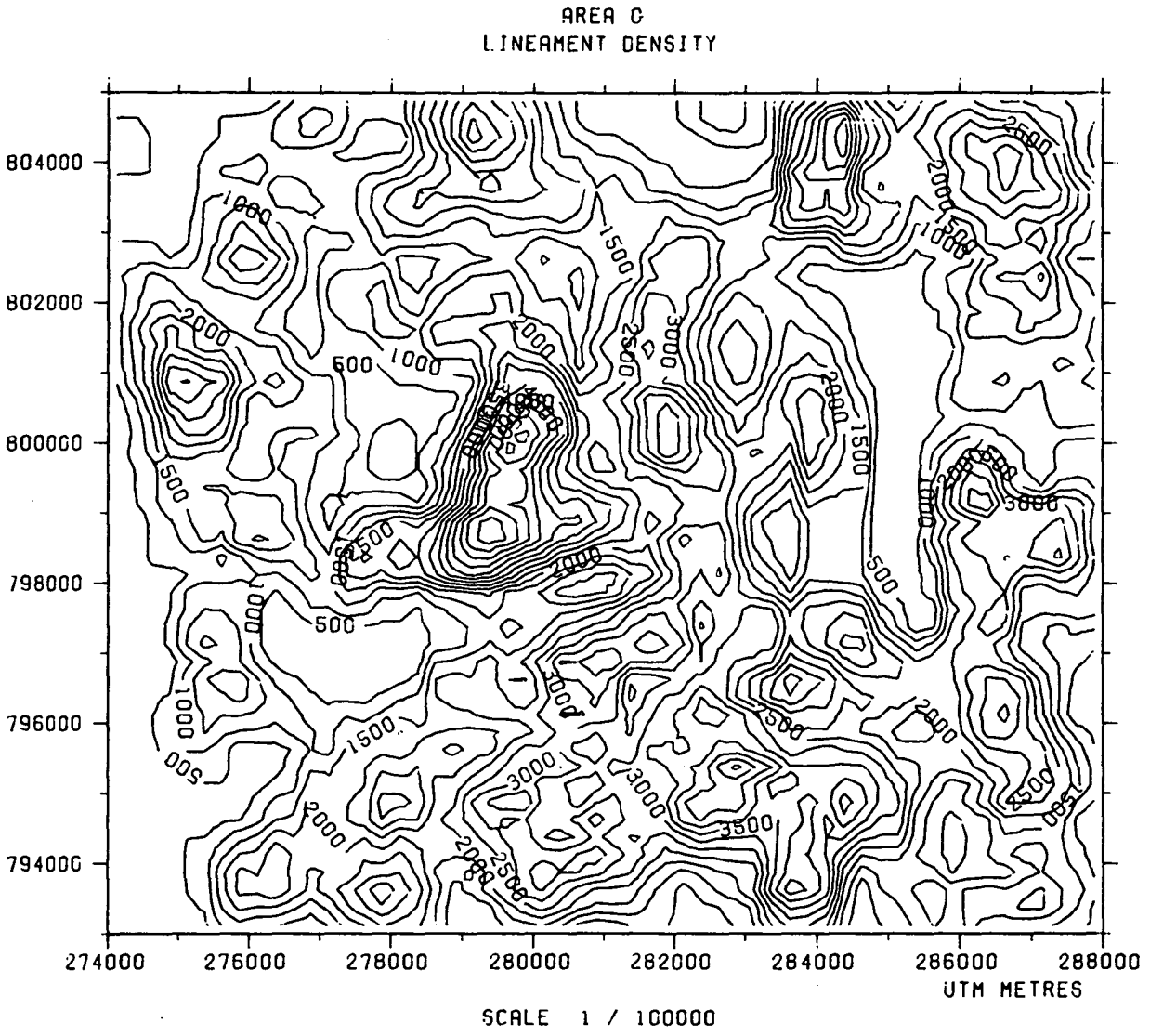
AREA C
LINEAMENT DENSITY
804000
802000
800000
798000
796000
794000
274000
276000
278000
280000
282000
284000
286000
288000
UTM METRES
SCALE 1 / 100000

Figure 3G

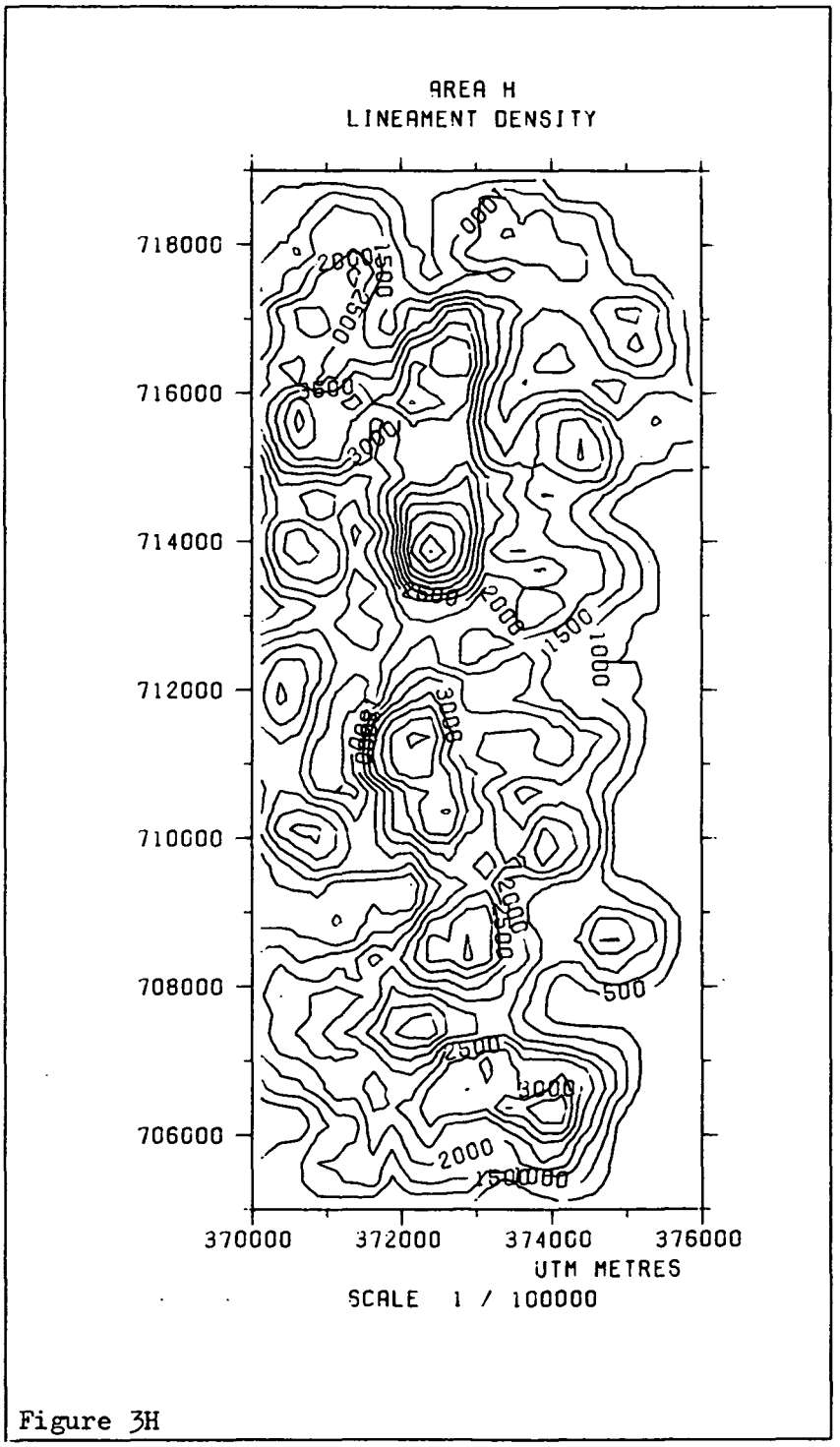
AREA H
LINEAMENT DENSITY
718000
716000
714000
712000
710000
708000
706000
370000
372000
374000
376000
UTM METRES
SCALE 1 / 100000

Figure 3H

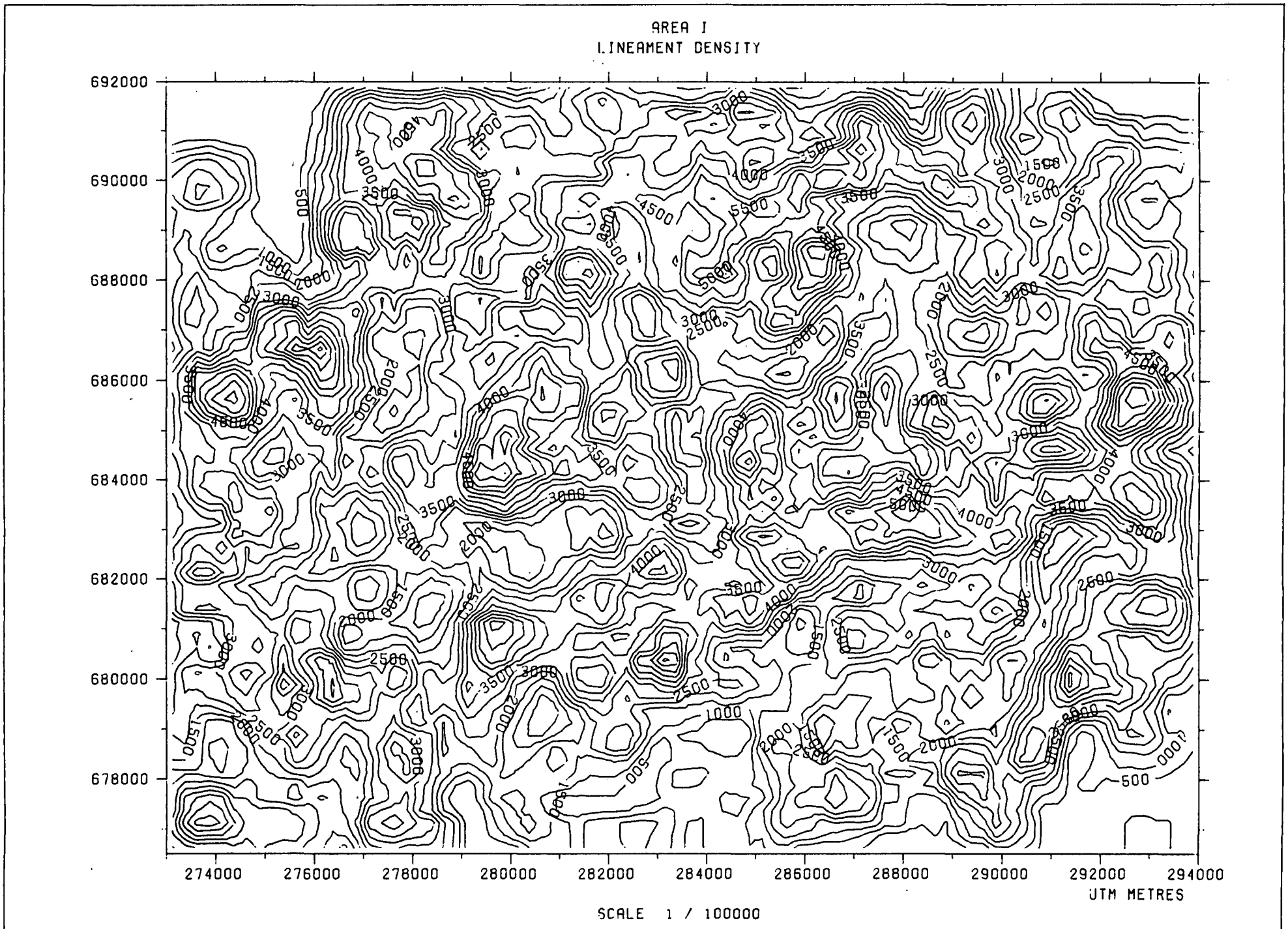
AREA I
LINEAMENT DENSITY
692000
690000
688000
686000
684000
682000
680000
678000
274000
276000
278000
280000
282000
284000
286000
288000
290000
292000
294000
UTM METRES
SCALE 1 / 100000

Figure 3I

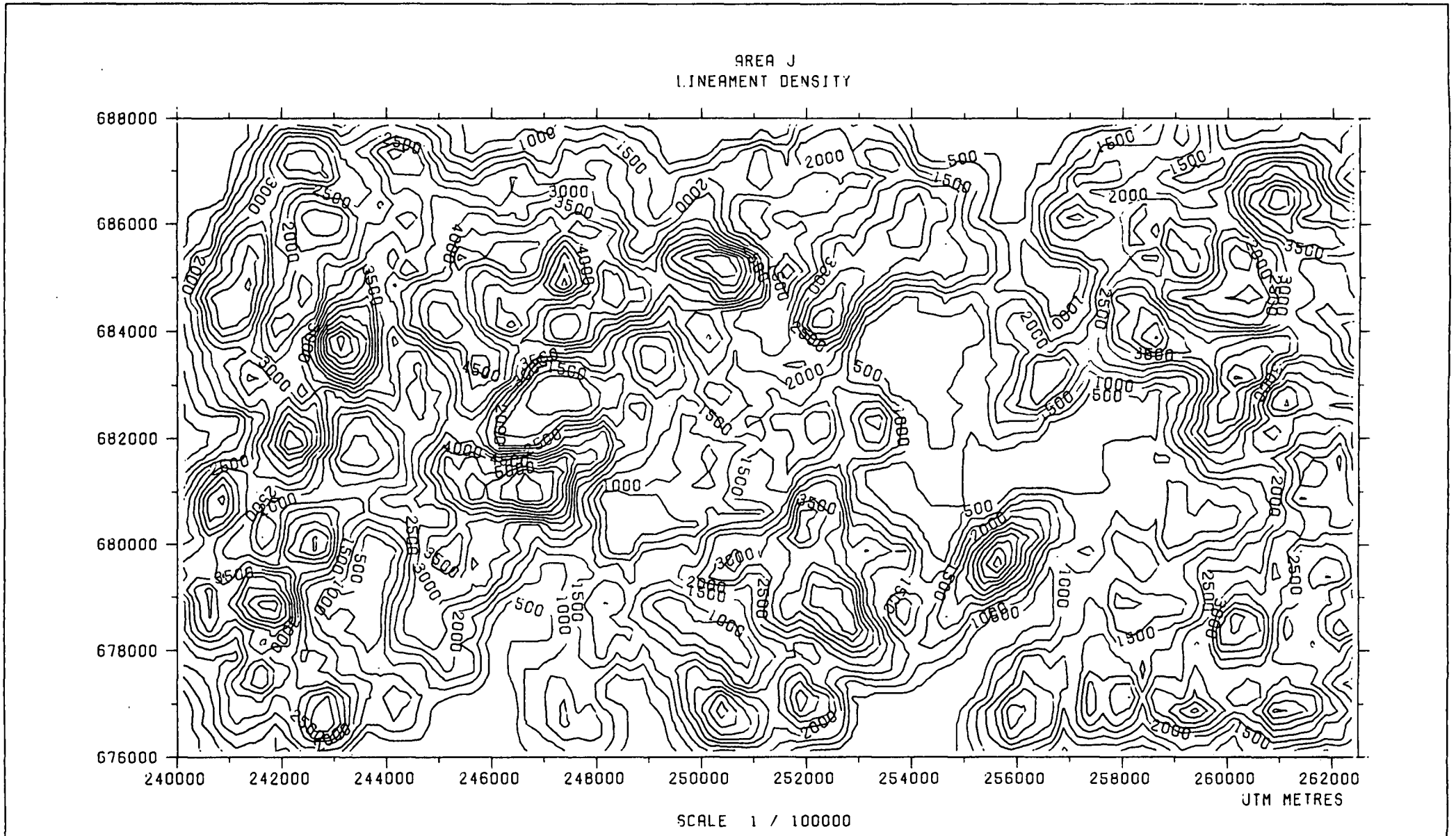
AREA J
LINEAMENT DENSITY
688000
686000
684000
682000
680000
678000
676000
240000
242000
244000
246000
248000
250000
252000
254000
256000
258000
260000
262000
UTM METRES
SCALE 1 / 100000

Figure 3J

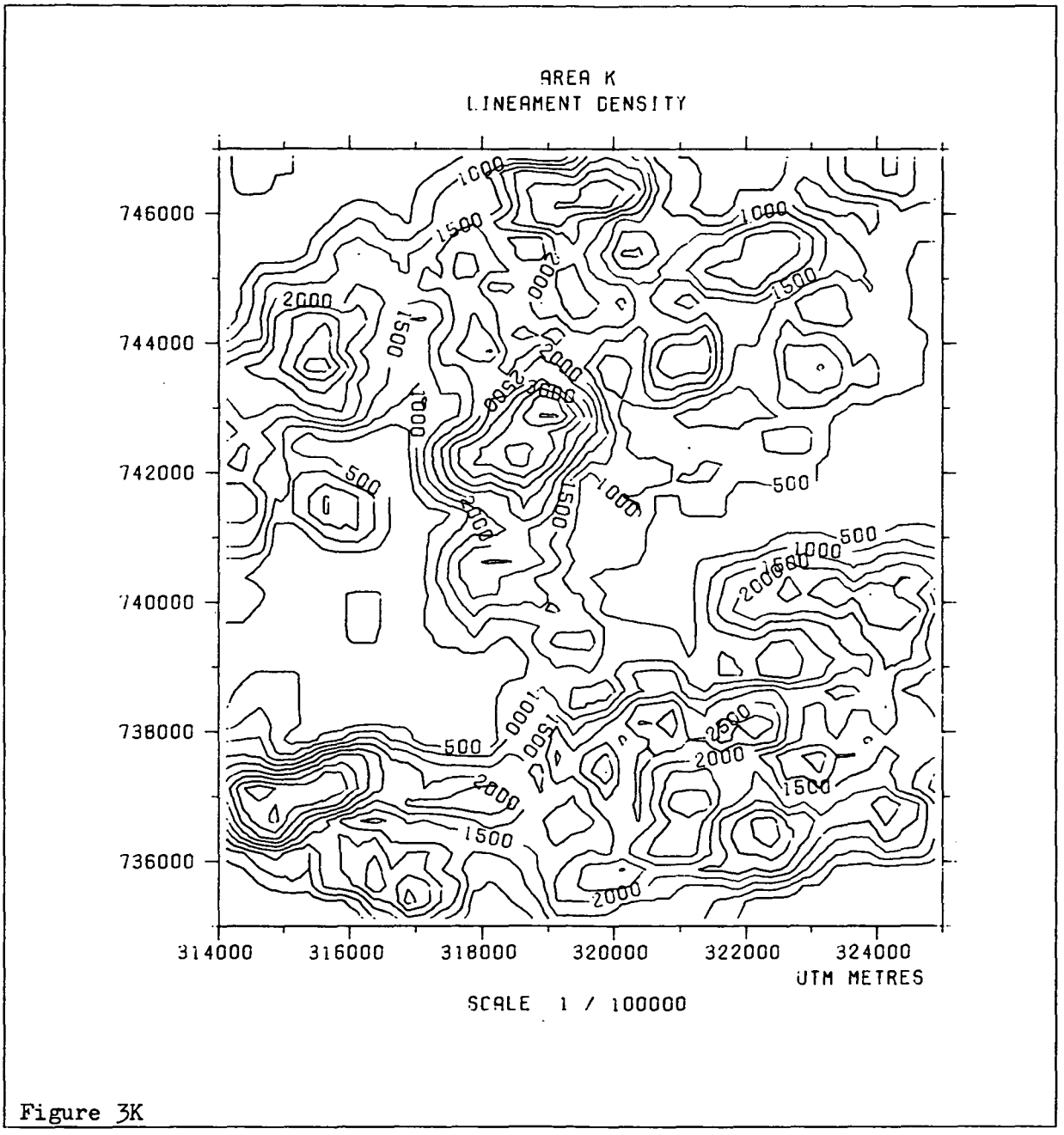
AREA K
LINEAMENT DENSITY
746000
744000
742000
740000
738000
736000
314000
316000
318000
320000
322000
324000
UTM METRES
SCALE 1 / 100000

Figure 3K

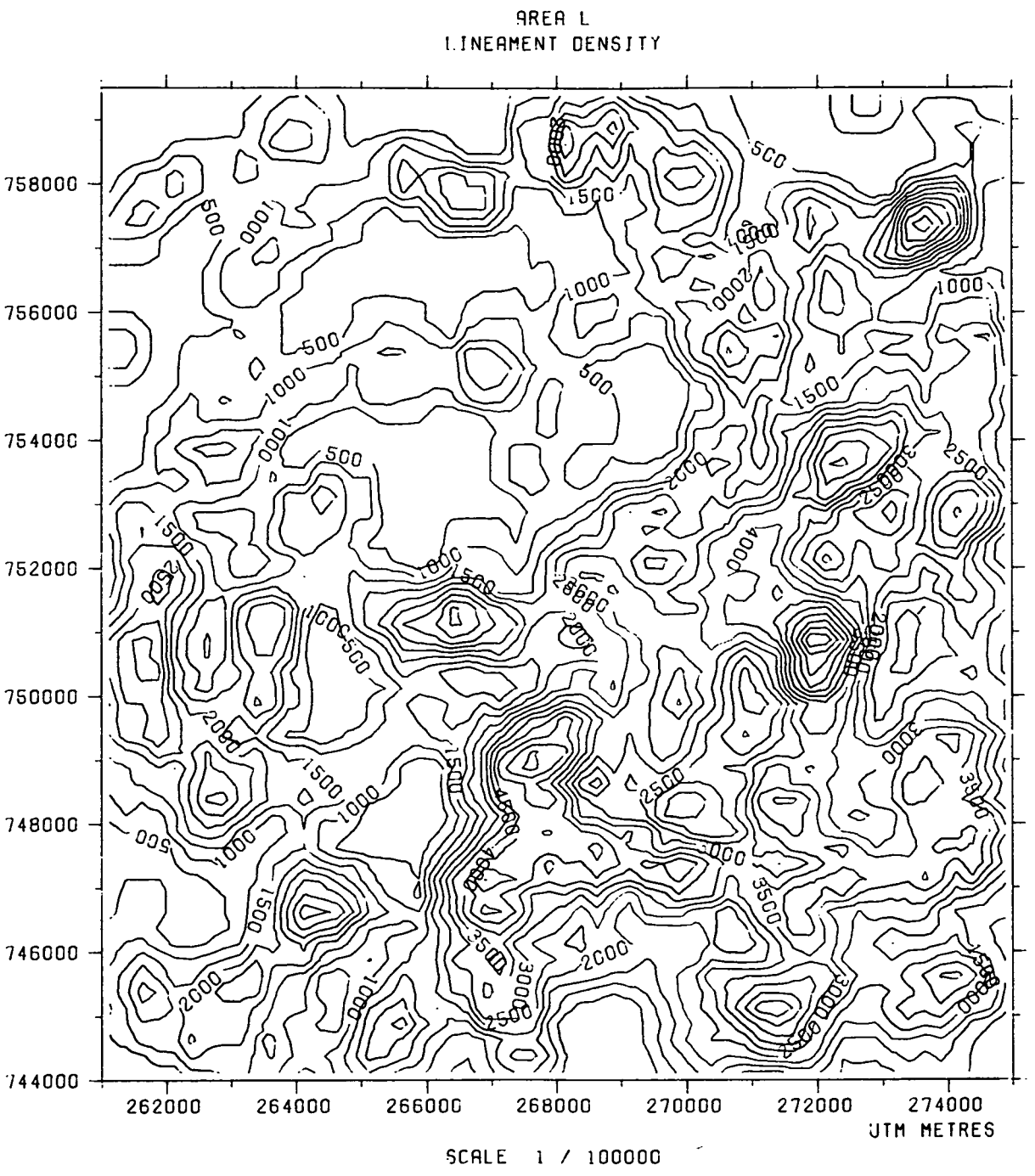
AREA L
LINEAMENT DENSITY
758000
756000
754000
752000
750000
748000
746000
744000
262000
264000
266000
268000
270000
272000
274000
UTM METRES
SCALE 1 / 100000

Figure 3L

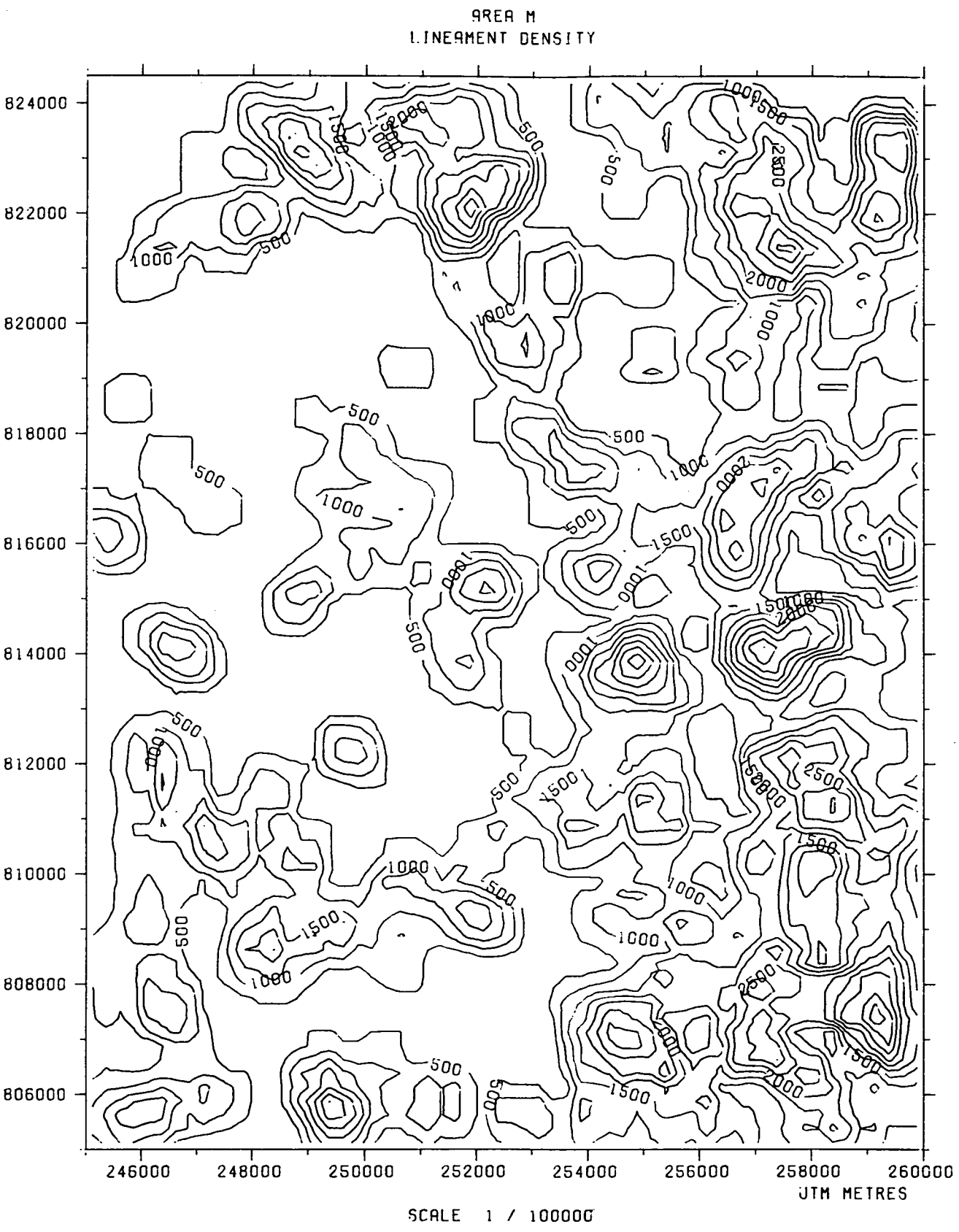
AREA M
LINEAMENT DENSITY
824000
822000
820000
818000
816000
814000
812000
810000
808000
806000
246000
248000
250000
252000
254000
256000
258000
260000
UTM METRES
SCALE 1 / 100000

Figure 3M

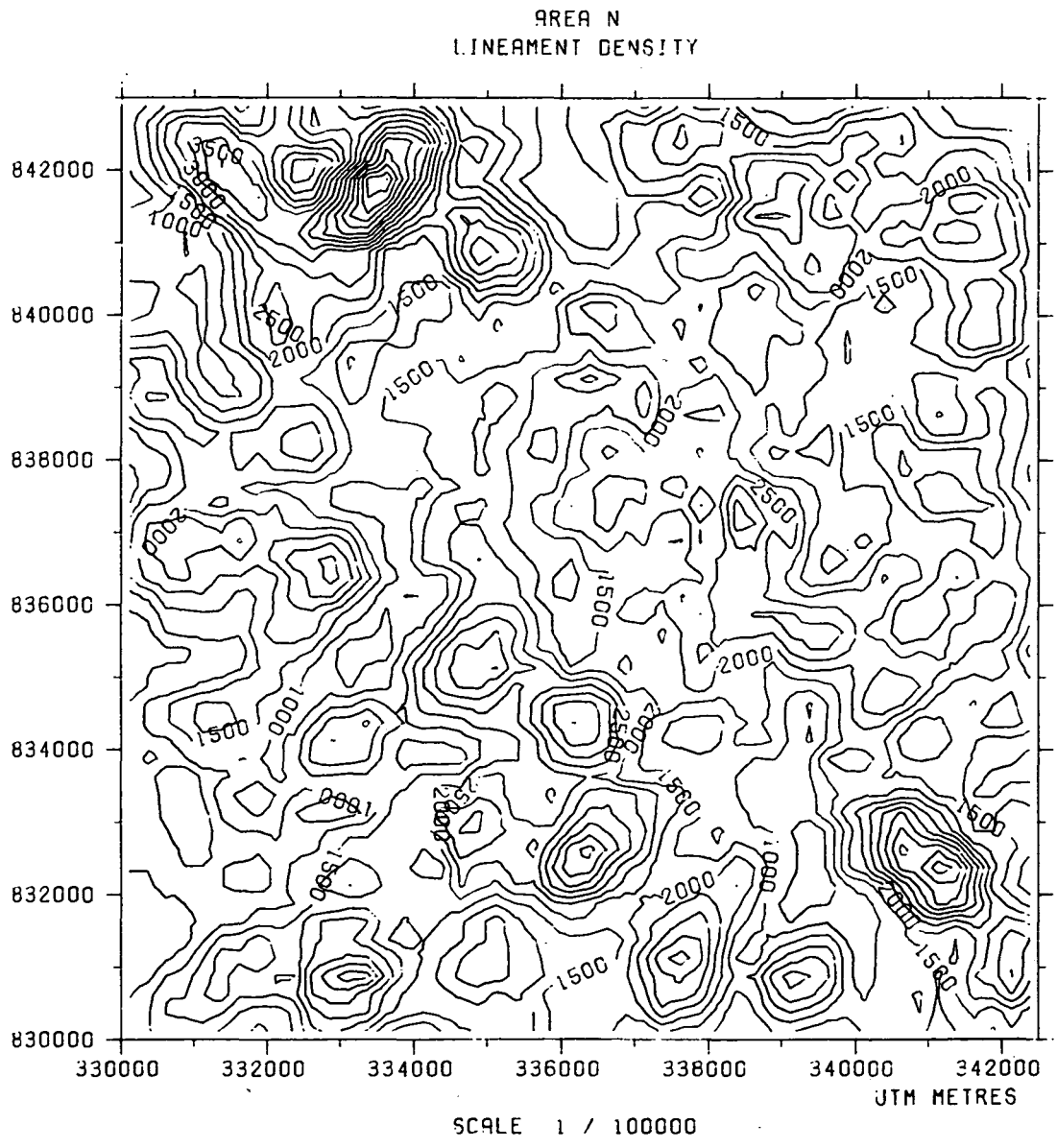
AREA N
LINEAMENT DENSITY
842000
840000
838000
836000
834000
832000
830000
330000
332000
334000
336000
338000
340000
342000
UTM METRES
SCALE 1 / 100000

Figure 3N

Figures 4A to N: Computer-generated rose diagrams for study areas A to N, using the lineament data in Figures 2A to N. A length-weighted calculation is used with a sector size of 10°. The scale factor on each plot is shown.

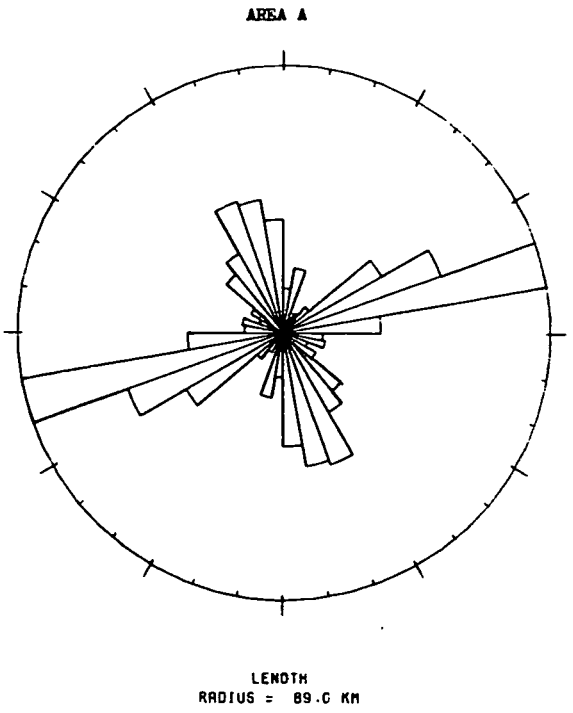

Figure 4A

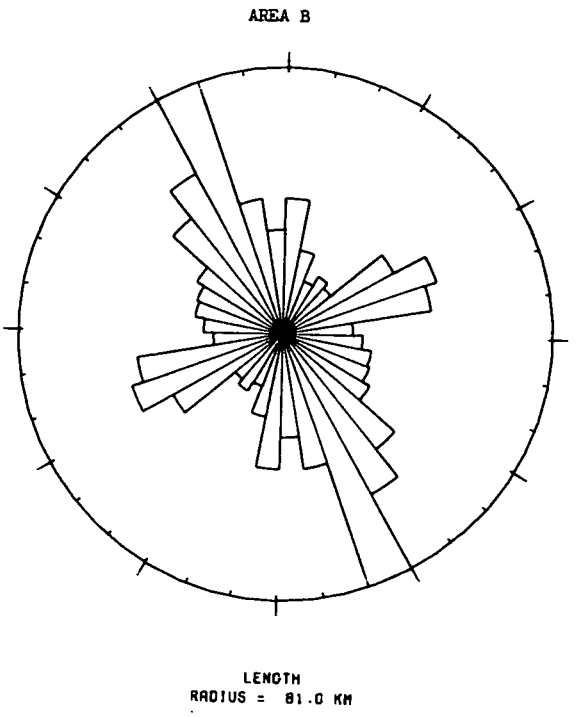

Figure 4B

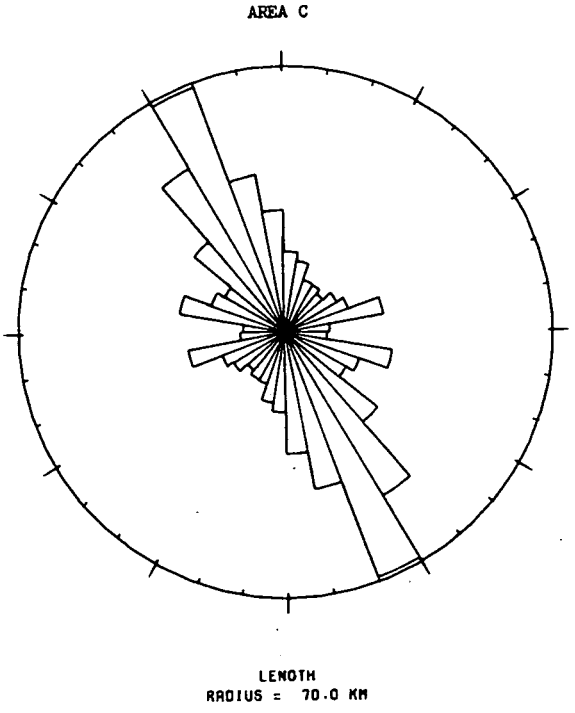

Figure 4C

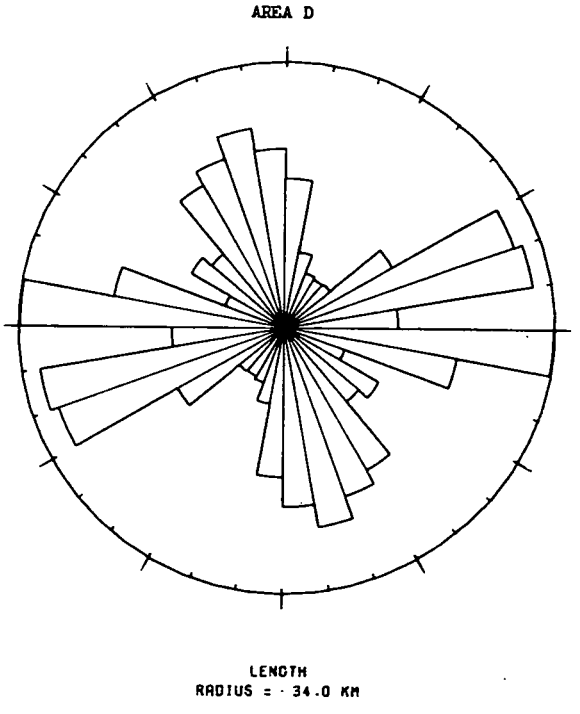

Figure 4D

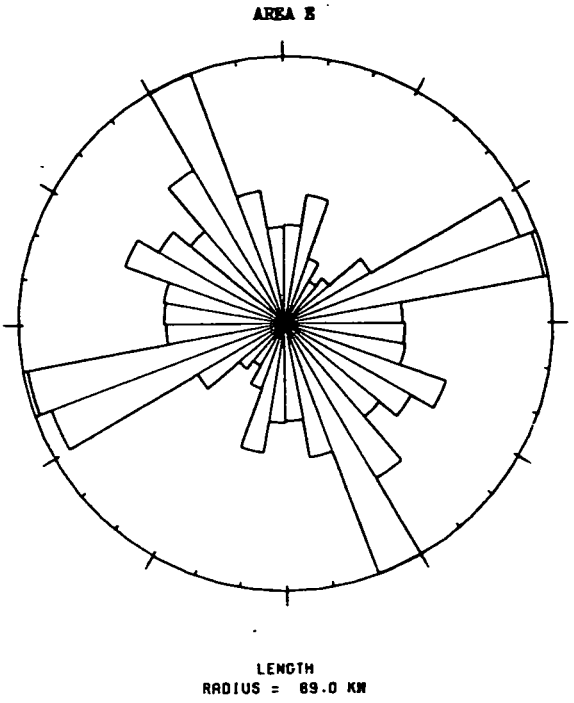

Figure 4E

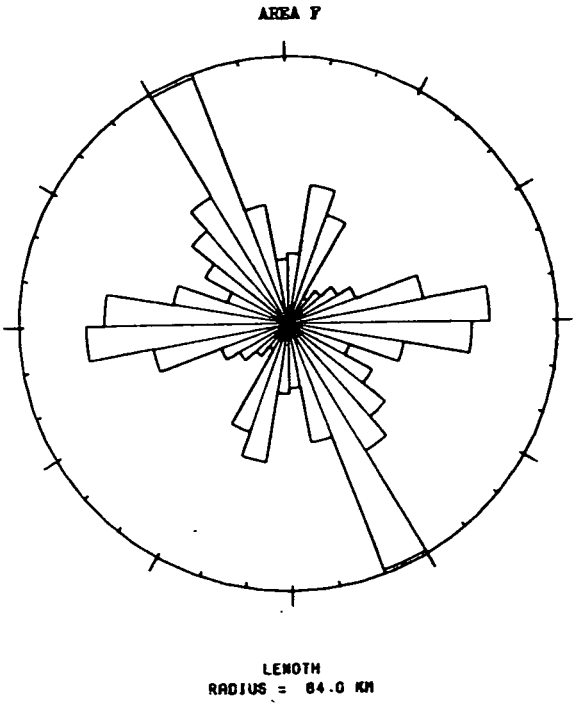

Figure 4F

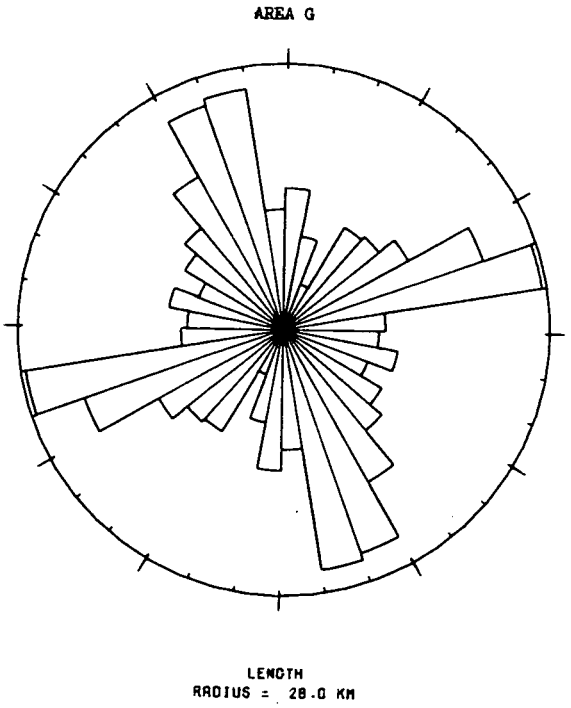

Figure 4G

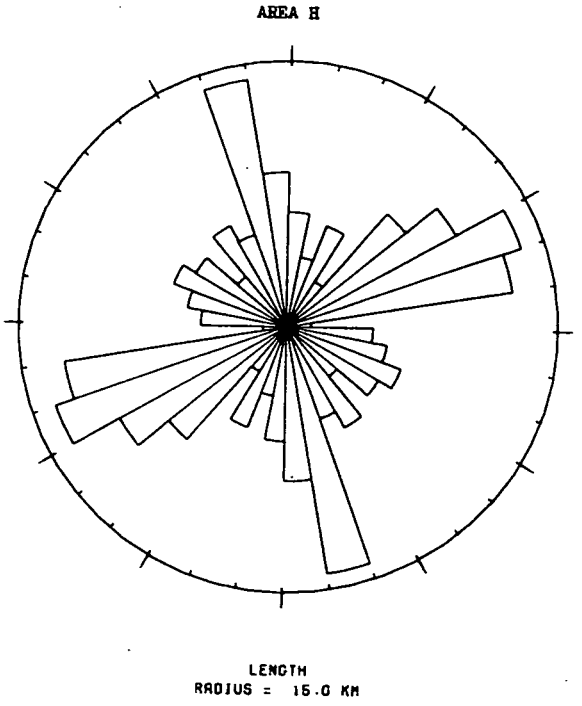

Figure 4H

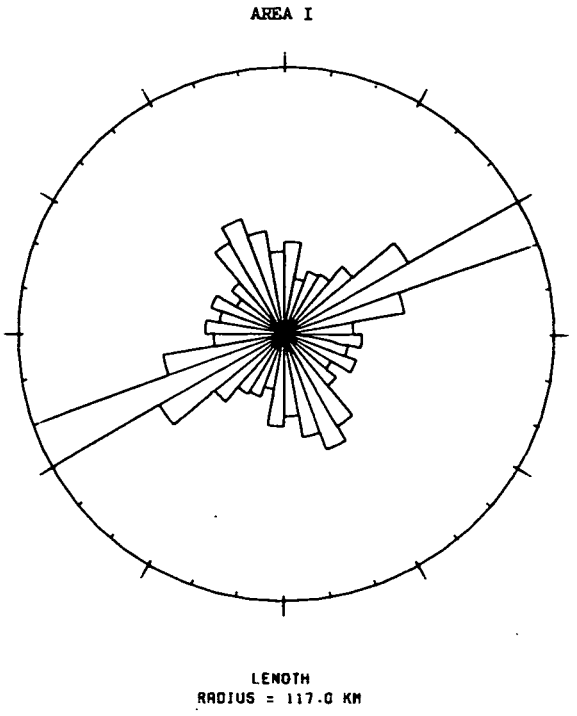

Figure 4I

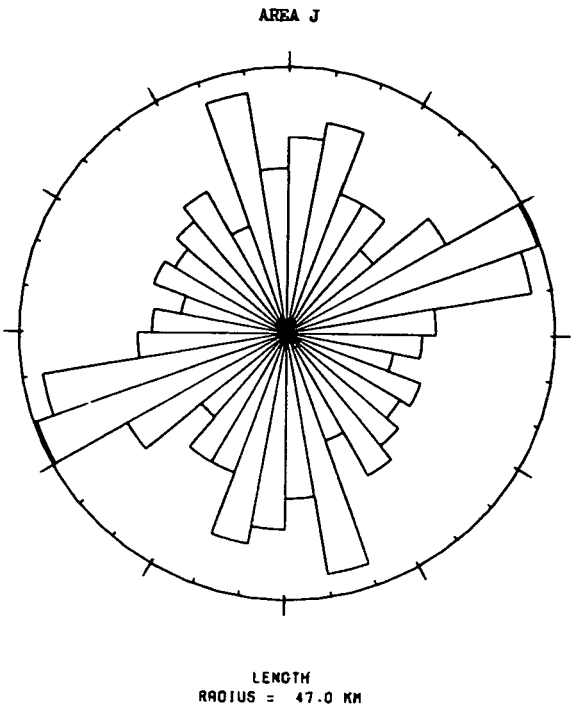

Figure 4J

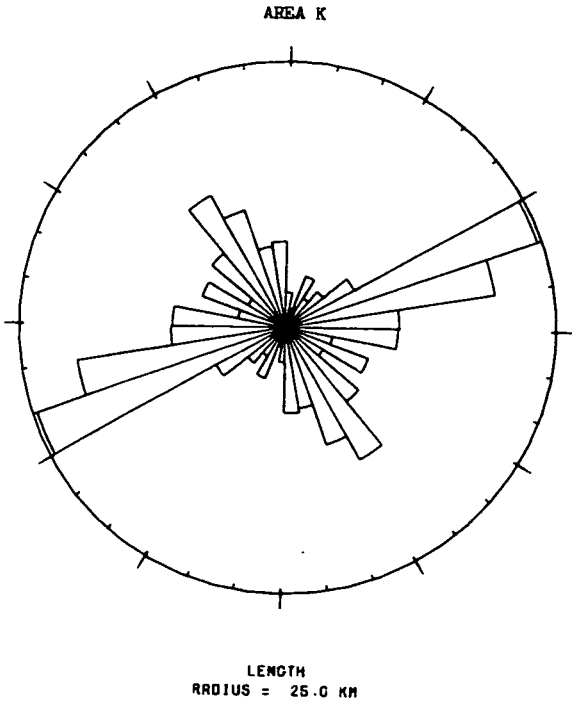

Figure 4K

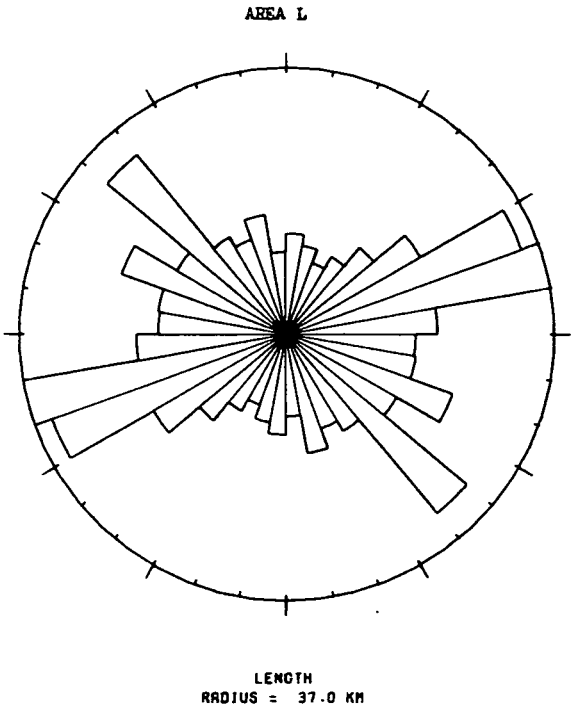

Figure 4L

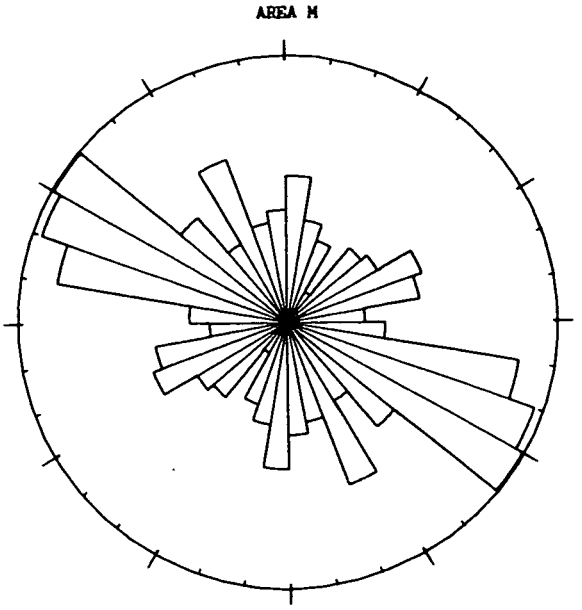

Figure 4M

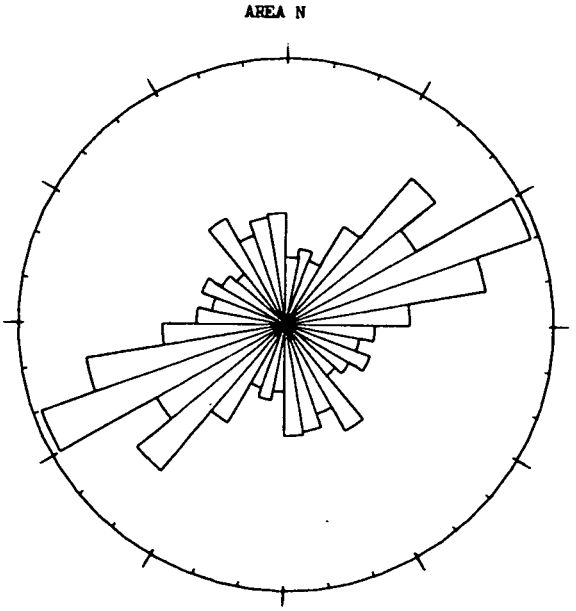

Figure 4N

Figures 5A and B: Computer-generated rose diagrams for the satellite-derived and summed-photolineament datasets respectively. Roses are based on a length-weighted calculation using a sector size of 5°. The scale factor on each plot is shown.

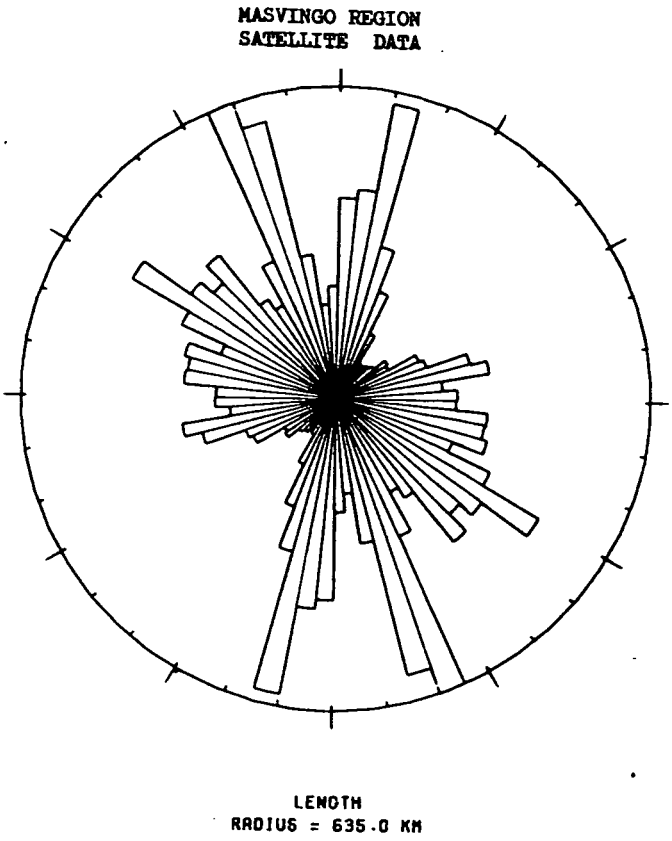

Figure 5A

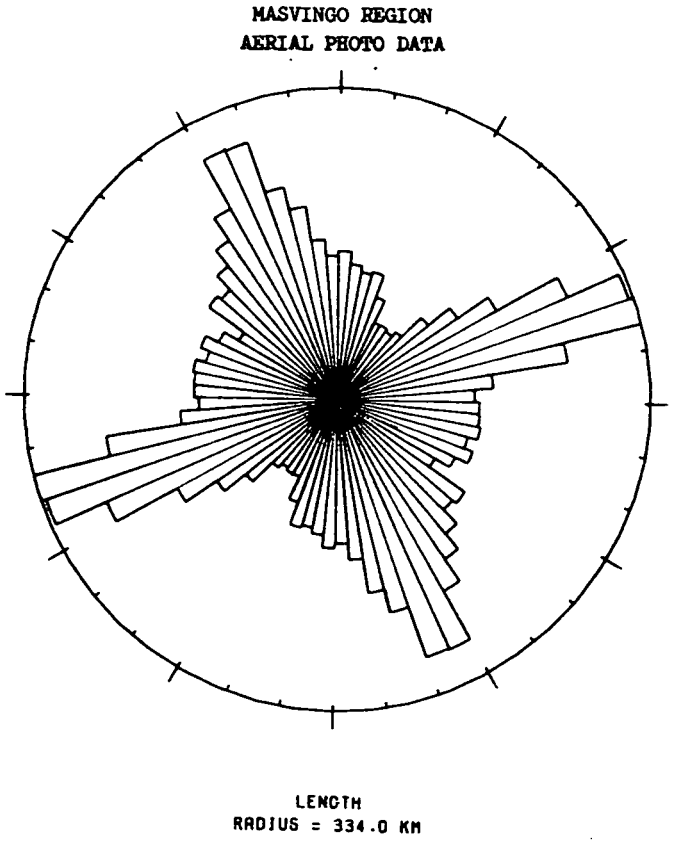

Figure 5B

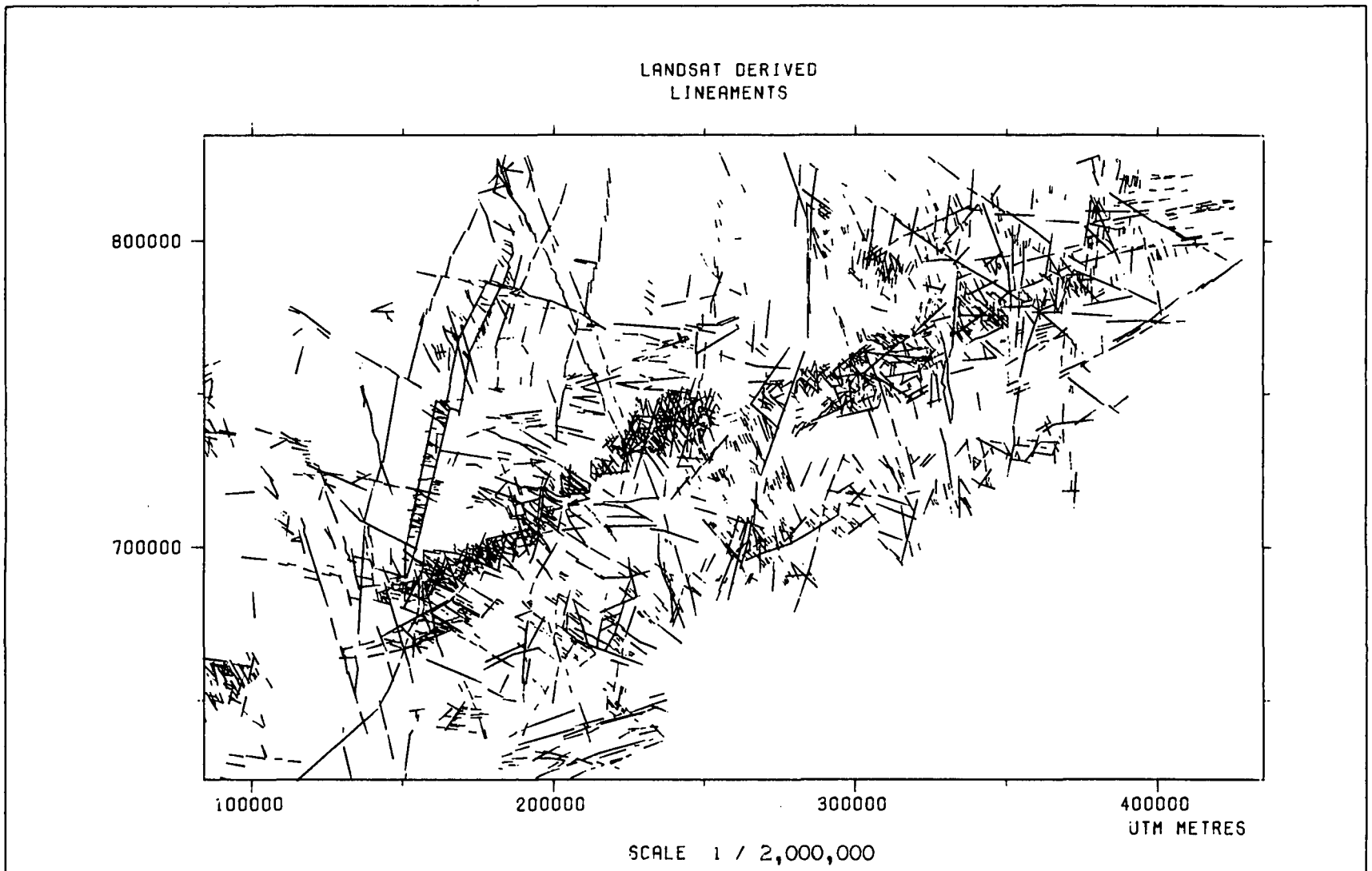
LANDSAT DERIVED
LINEAMENTS
800000
700000
100000
200000
300000
400000
UTM METRES
SCALE 1 / 2,000,000

Figure 6

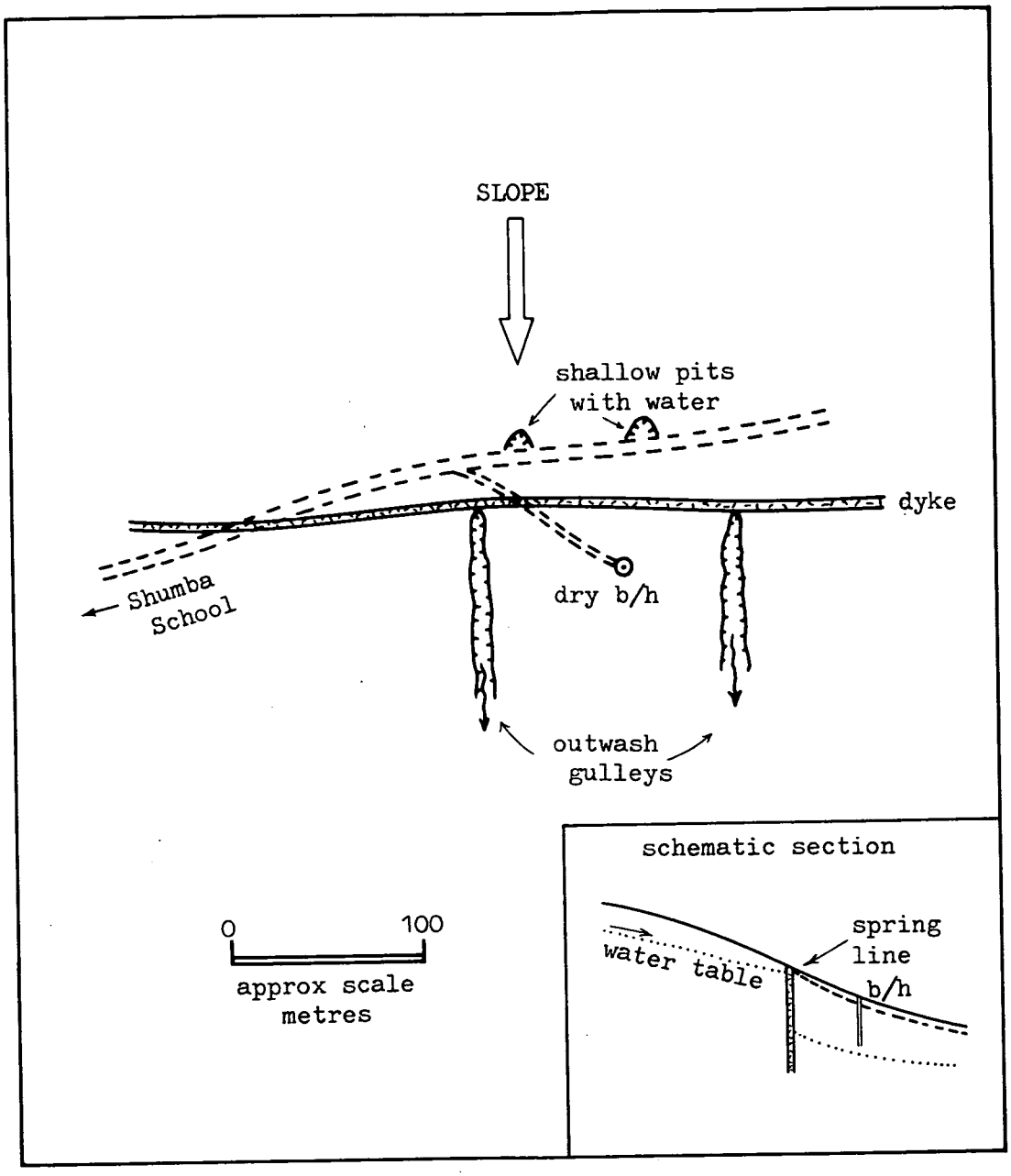

Figure 7: Sketch map to illustrate relationships near Shumba School, Area E. Here, a dolerite dyke appears to act as a sub-surface barrier to groundwater flow.

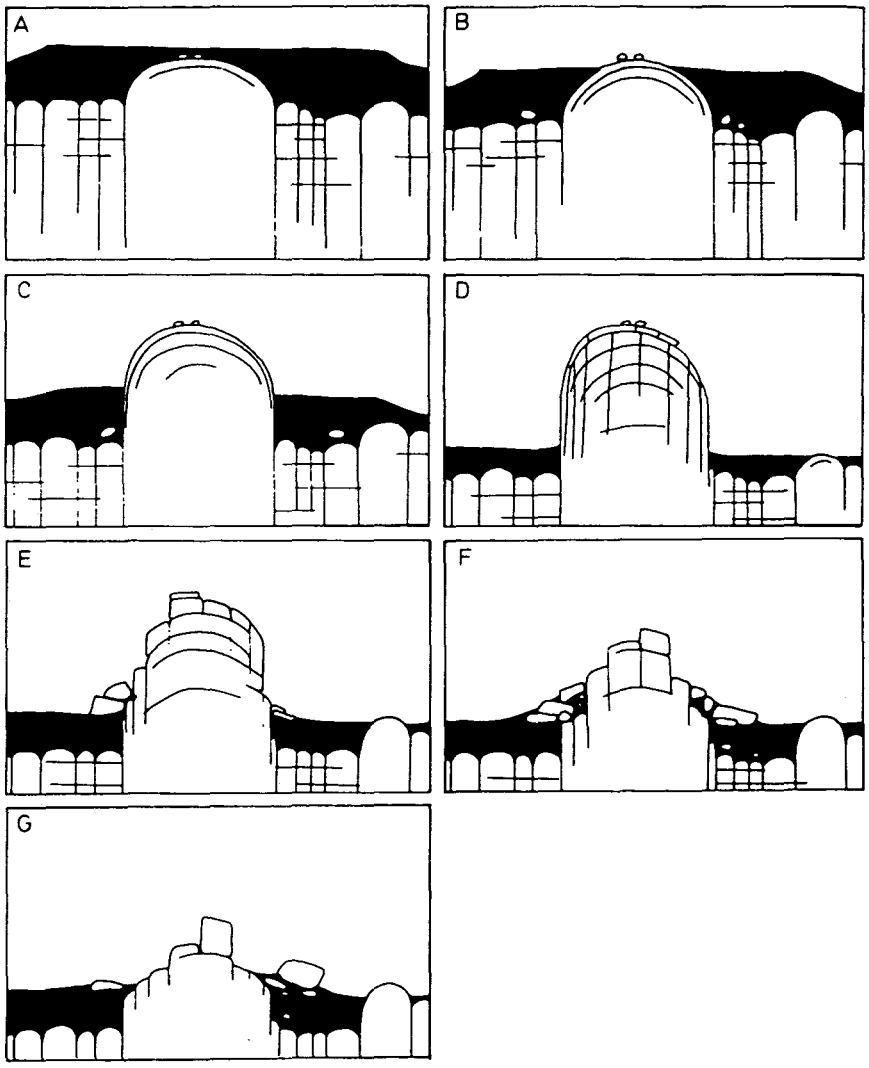

Figure 8: The evolution of bornhardts according to Thomas (1965). Each phase of regolith stripping is accompanied by further lowering of the basal surface of weathering around the bornhardt. In this way, the dome height may eventually exceed the original depth of the weathering profile (from Ollier 1984).

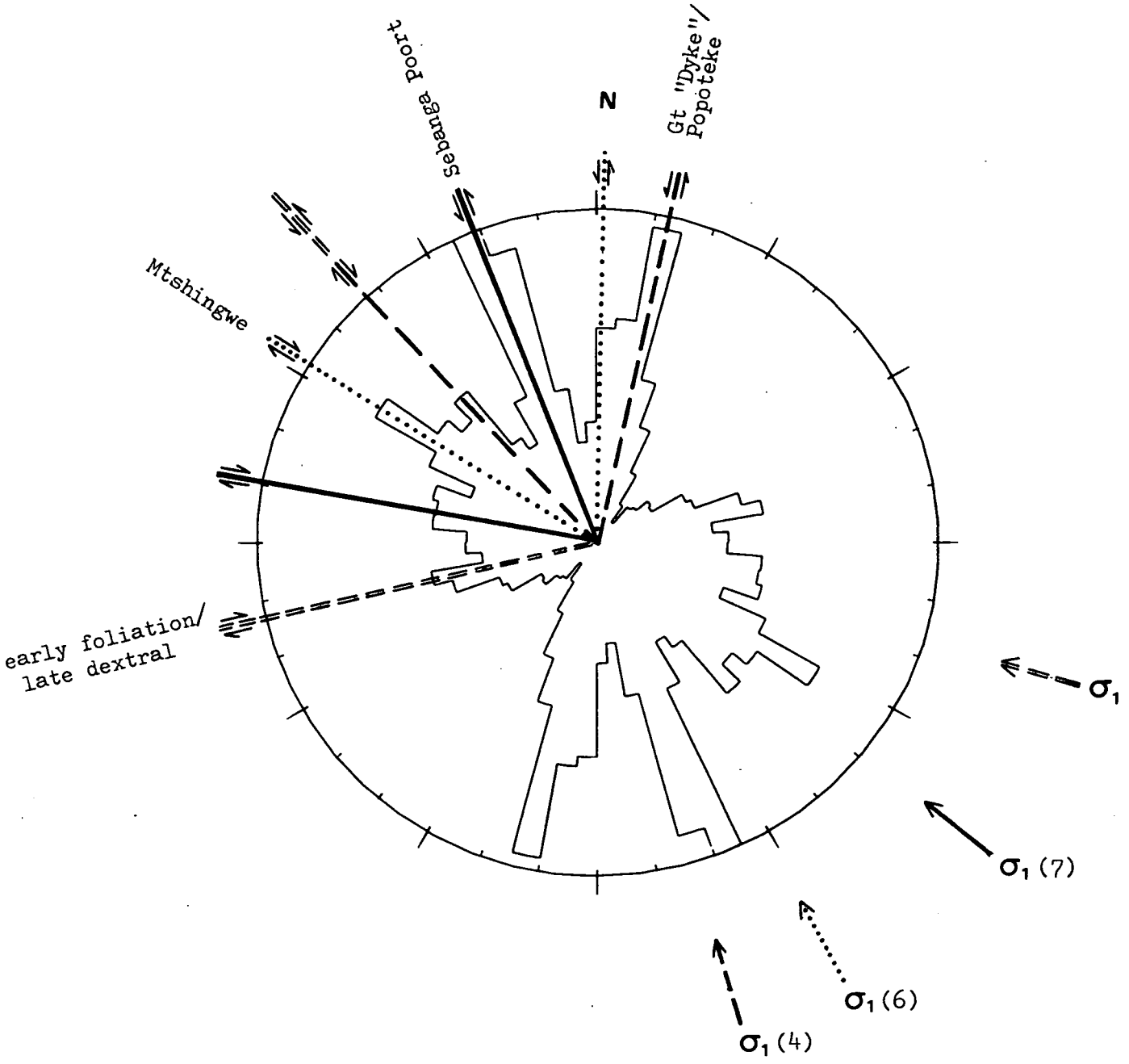

Figure 9: Interpreted conjugate fracture sets on length-weighted rose diagram of the satellite lineament dataset indicating a progressive rotation of the maximum horizontal principal stress axis from event (4) to event (9) [Table 1].

Plate 1: Development of open joint along mineral foliation plane in outcrop of the Zimbabwe Granite [area A].

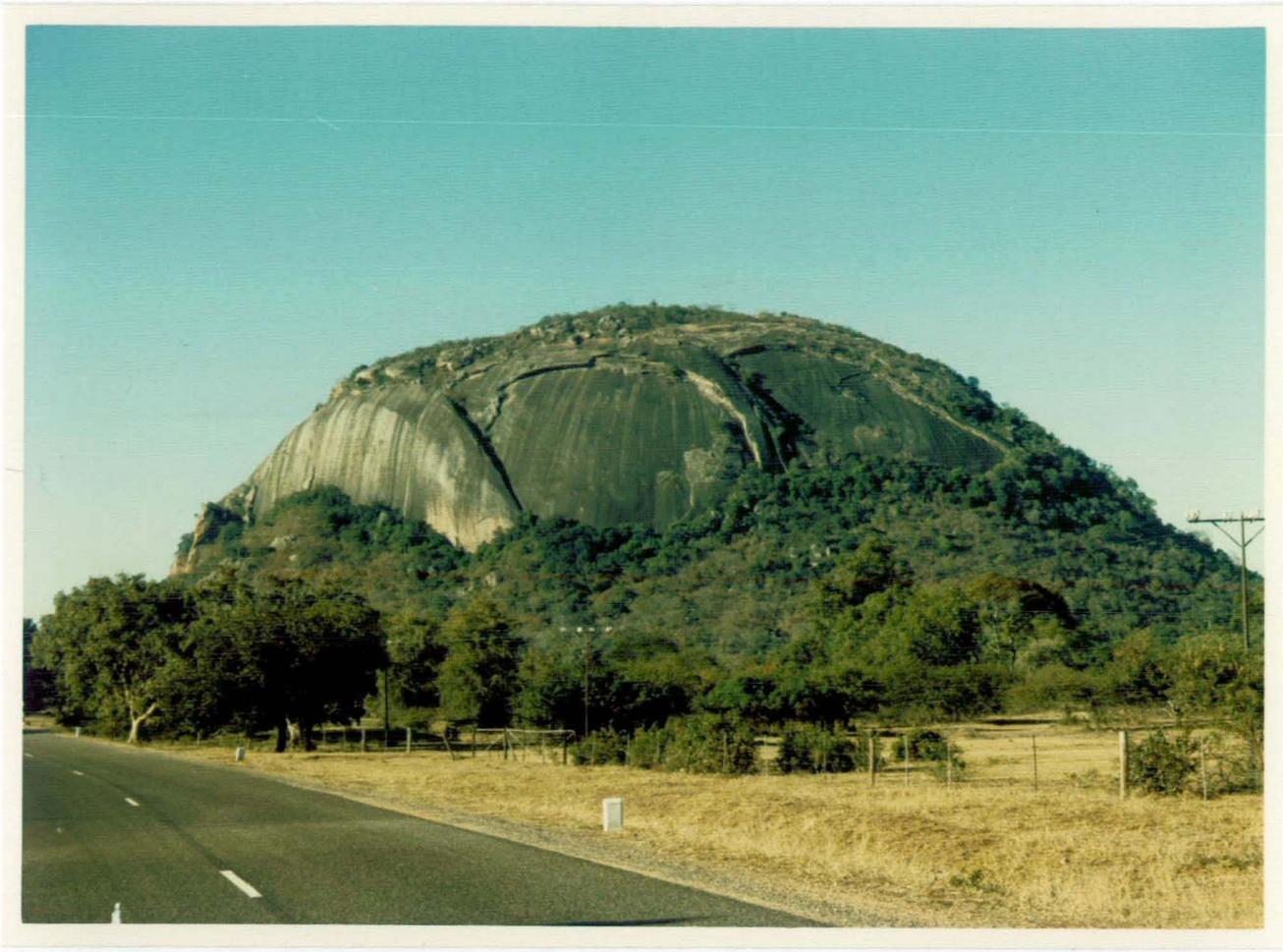

Plate 2: Domal bornhardt in massive, porphyritic granite showing sheet exfoliation [area B].

Plate 3: Rubbly outcrop along dolerite dyke and associated vegetation line [area E].

Plate 4: Planar vertical joints on bornhardt outcrop within the Chibi Granite. Two of the three directions visible form an apparent conjugate set, but no movement is evident across pegmatite veins [area F].

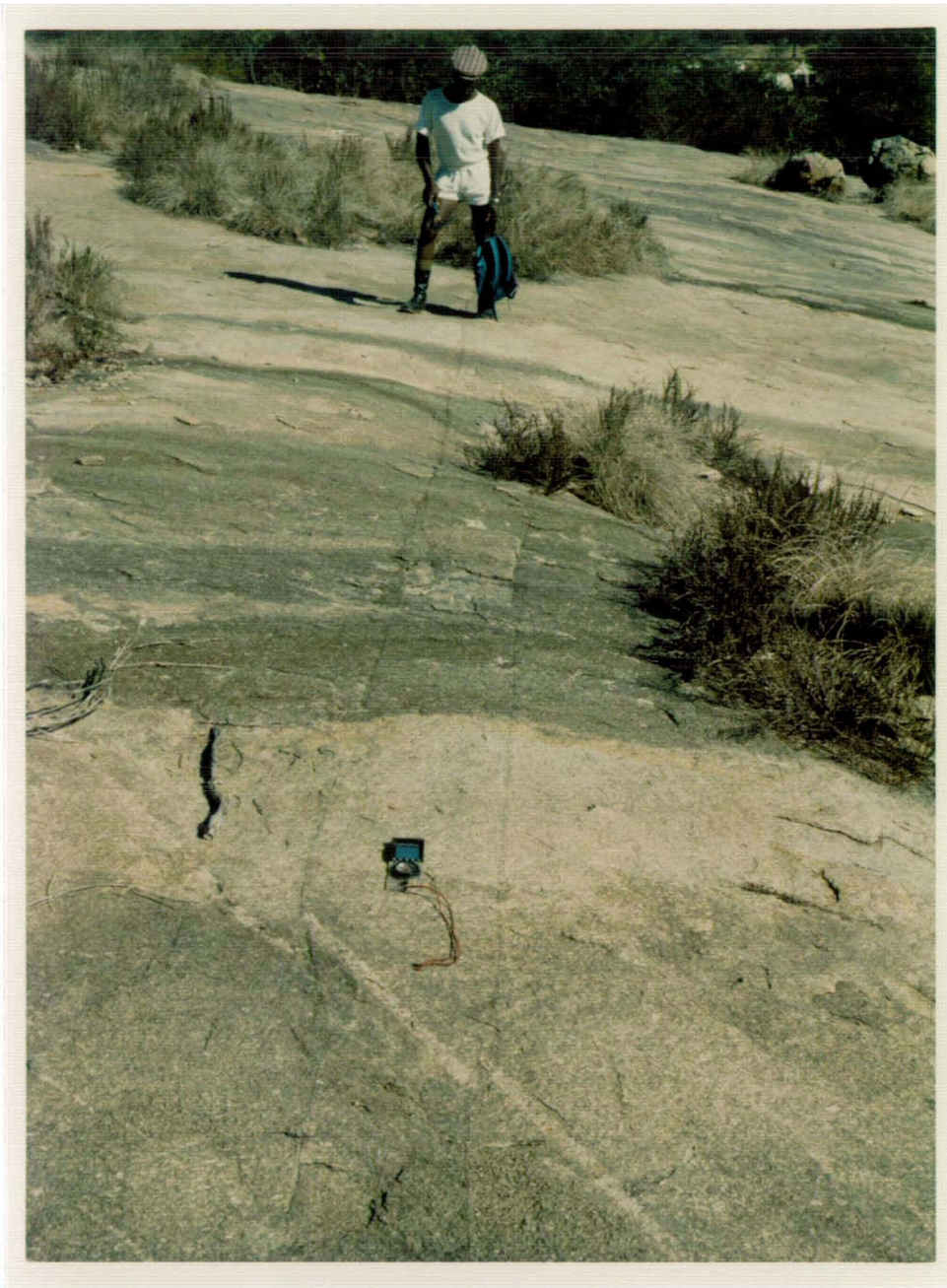

Plate 5: Minor, quartz-filled, sinistral strike-slip faults cutting the Chibi Granite [near Davira B.C.]. The fractures trend NNE and are part of the Popoteke faulting event.

Plate 6: Young, planar, vertical joints in younger granite at the Masvingo Quarry. The joints open as quarrying proceeds as a result of the lateral pressure release. A network of vertical and sub-horizontal joints can be seen on the quarried face in the background.